

Geological Society of America Bulletin

Physical volcanology of the post–twelfth-century activity at Cotopaxi volcano, Ecuador: Behavior of an andesitic central volcano

Marco Pistolesi, Mauro Rosi, Raffaello Cioni, Katharine V. Cashman, Andrea Rossotti and Eduardo Aguilera

Geological Society of America Bulletin 2011;123, no. 5-6;1193-1215
doi: 10.1130/B30301.1

Email alerting services

click www.gsapubs.org/cgi/alerts to receive free e-mail alerts when new articles cite this article

Subscribe

click www.gsapubs.org/subscriptions/ to subscribe to Geological Society of America Bulletin

Permission request

click <http://www.geosociety.org/pubs/copyrt.htm#gsa> to contact GSA

Copyright not claimed on content prepared wholly by U.S. government employees within scope of their employment. Individual scientists are hereby granted permission, without fees or further requests to GSA, to use a single figure, a single table, and/or a brief paragraph of text in subsequent works and to make unlimited copies of items in GSA's journals for noncommercial use in classrooms to further education and science. This file may not be posted to any Web site, but authors may post the abstracts only of their articles on their own or their organization's Web site providing the posting includes a reference to the article's full citation. GSA provides this and other forums for the presentation of diverse opinions and positions by scientists worldwide, regardless of their race, citizenship, gender, religion, or political viewpoint. Opinions presented in this publication do not reflect official positions of the Society.

Notes



Physical volcanology of the post–twelfth-century activity at Cotopaxi volcano, Ecuador: Behavior of an andesitic central volcano

Marco Pistolesi^{1†}, Mauro Rosi¹, Raffaello Cioni², Katharine V. Cashman³, Andrea Rossotti⁴, and Eduardo Aguilera⁵

¹*Earth Science Department, University of Pisa, Santa Maria, 53, Pisa, Pisa 56126, Italy*

²*Earth Science Department, University of Cagliari, Trentino, 51, Cagliari, Cagliari 09127, Italy*

³*Department of Geological Sciences, University of Oregon, 1244 Walnut Street, Eugene, Oregon 97403-2056, USA*

⁴*Cucchiari, 29, Milano, Milano 20155, Italy*

⁵*Escuela Politécnica del Ejército (ESPE), General Rumiñahui, Sangolquí 171-5-231B, Ecuador*

ABSTRACT

Cotopaxi volcano, situated in the Eastern Cordillera of the Ecuadorian Andes, is one of the most active volcanoes on Earth. The volcano is well known for the magnificence of its almost perfectly symmetrical cone topped by ice and snow and for the destructive power of its large-scale, syneruptive lahars. This paper presents a stratigraphic study of the post–twelfth-century eruptive products that reveals the existence of 21 continuous tephra beds. Most of them were characterized from both a physical (dispersal areas, deposit volumes, peak Mass Discharge Rate [MDR] of the eruptions) and compositional point of view. New ¹⁴C dates, linked with a new examination of historical chronicles, allow us to create a new chronostratigraphic scheme for this period of activity, which is bracketed by the emplacement of a regional tephra marker (A.D. 1140 ash bed from Quilotoa volcano) and the present day. The first period (A.D. 1150–1742) included only two moderate-intensity explosive eruptions, the oldest being possibly related to a dome disruption. In contrast, the period A.D. 1742–1880 started with two high-intensity, Plinian eruptions (maximum column heights of 25 and 29 km), followed by several short-lived but sustained, convective episodes. Deposits of pyroclastic surges and scoria flows were emplaced during some of these short-lived events and may have been related to column collapse and boiling over activity, respectively. Post-1880 activity, reported in 1904, 1906, and 1912, likely consisted of minor explosions that affected only the crater area.

Our study of recent activity at Cotopaxi shows that high dispersive power (peak mass discharge rates from 1.1 to 9.3 × 10⁷ kg/s) is associated with the eruption of only moderate amounts of magma (1.1 × 10¹⁰–6.0 × 10¹¹ kg, or ~0.005–0.2 km³ Dense Rock Equivalent [DRE]). Additionally, although the past 2000 yr of activity at Cotopaxi have been interpreted to reflect a fairly uniform magma supply rate, detailed analysis of the past centuries, and a reanalysis of data from the past 2000 yr show that Cotopaxi's eruptive activity is characterized by clusters of eruptive events that are separated by periods of long quiescence punctuated by isolated eruptions, often of slightly more evolved magma.

No systematic variations in composition emerge in the time sequence. Although new magmatic phases commonly start with the eruption of mafic magma, this is not always observed. Additionally, eruption clusters may show either compositional trends of increasing SiO₂ content or abrupt compositional changes within a cluster. We interpret the temporal and compositional variations in eruptive activity to reflect the complex interplay of deep versus shallow magmatic processes. An important result from the perspective of volcanic hazards is our conclusion that, over the studied period, no clear relation exists among repose time, eruption magnitude, and magma composition. This conclusion contrasts with the periodic eruptive behavior that has been postulated at many central volcanoes worldwide, thus inviting a reexamination of other intermediate-composition volcanic

systems and a reassessment of the assumption of periodic activity.

INTRODUCTION

Recent studies of frequently erupting basaltic volcanoes have demonstrated important temporal variations in the rates of magma supply from deeper to shallower levels. For example, studies of Kilauea, Etna, Krafla, and Piton de la Fournaise volcanoes show that the magma supply rate varies significantly over time periods of decades to centuries (Dvorak and Dzurisin, 1993; Wadge et al., 1975; Takada, 1999; Andronico and Lodato, 2005; Vlastélic et al., 2009). However, although inputs of mafic magma are commonly invoked as eruptive triggers in intermediate and silicic systems (e.g., Sigurdsson and Sparks, 1978; Eichelberger et al., 2006; Di Muro et al., 2008b; Kratzmann et al., 2009; Humphreys et al., 2010), the extent to which these systems are also characterized by variations in the rates of magma supply and magma discharge, and the range of time scales of such variations are poorly constrained.

Petrologic and geochronologic studies of intermediate-composition stratovolcanoes show that they are typically long-lived and are constructed in spurts that indicate variations in magma discharge over tens of thousands of years (e.g., Hildreth and Lanphere, 1994; Bacon and Lanphere, 2006). Detailed physical volcanological studies of past activity at single central volcanoes, such as Oshima volcano, Japan (Nakamura, 1964), Mount St. Helens, USA (Crandell, 1987; Mullineaux and Crandell, 1981), and Vesuvius, Italy (e.g., Cioni et al., 2008), suggest that stratovolcano activity may

[†]E-mail: pistolesi@dst.unipi.it

also be episodic over shorter time scales. New models use these studies as a starting point to relate processes in the lower crust to observed pulses in volcanic activity of deep crustal hot zones (e.g., Annen et al., 2006), and to refine volcanic hazard assessments (e.g., Cioni et al., 2008; Neri et al., 2008). Such detailed studies of processes within a single volcanic system are limited, however, because of problems of sufficient exposures (particularly for older material), problems in dating, and difficulties in relating proximal flows (pyroclastic flows, lava flows, and lahars) to distal fall deposits.

In this paper, we combine detailed mapping and field measurements with examination of historical chronicles to develop a detailed eruptive chronology of the past eight centuries for Cotopaxi volcano (Ecuador). The field study was facilitated by good access to the volcano's flanks, absence of vegetation cover, limited alteration of tephra, and by the superb exposure of all volcanic products. Our stratigraphic reconstruction, developed by examining more than 450 sites distributed around the volcano, allowed us to identify and trace 21 main tephra beds organized in plane-parallel successions separated by erosional unconformities. Cross-checking with the available chronicles and historical documents enabled us to relate most of the tephra units to documented volcanic events that have occurred since the Spanish conquest. The chronological framework was strengthened by four ^{14}C dates. Each tephra unit was characterized through grain-size and component analyses, measurement of maximum clast size, and compositional analysis of the juvenile fraction. Isopach and maximum clast dispersal maps (isopleths) of fallout deposits were compiled to assess the main physical volcanological parameters (volume, column height, and mass discharge rate) of the main eruptive episodes.

We demonstrate that, over the last eight centuries, eruptive activity at Cotopaxi volcano has not been regularly spaced in time. Additionally, we show that vigorous recharge of the system by a mafic (and likely volatile-rich) magma in the eighteenth century reinvigorated the system after a period of infrequent eruptive activity between the thirteenth and eighteenth centuries. The new magma influx produced repeated Plinian pulses followed by long-lived phases of substantial degassing and a series of sub-Plinian eruptions. Furthermore, the critical review of previously collected data (Barberi et al., 1995) suggests that a nonuniform magma supply rate has characterized at least the past 2000 yr of activity at Cotopaxi. Our study of this particular volcano thus invites reexamination of other intermediate-composition volcanic systems and

reassessment of assumptions of periodic activity for hazard assessment.

SUMMARY OF COTOPAXI'S EVOLUTION

Volcanism in Ecuador is characterized by volcanic activity that is dispersed both trenchward and behind the volcanic arc because of the structure of the subducting oceanic plate, which is carrying an aseismic ridge, the Carnegie Ridge, produced by the passage of the Nazca plate over the Galapagos hotspot. The surface expression of the corresponding active volcanic arc is broad (≤ 110 km; Bourdon et al., 2003) and consists of three different volcanic chains (Fig. 1): the volcanic front of the Western Cordillera (forearc position), the Eastern Cordillera (main arc position), and the Andean foothill (backarc position). The Inter-Andean Valley, a structural depression where Cotopaxi volcano is located, lies between the two Cordilleras (Fig. 1).

Geological and petrological descriptions of Cotopaxi extend back to the eighteenth century in a series of scientific monographs by La Condamine (1751), von Humboldt (1837–1838), Reiss (1874), Sodiro (1877), Stübel (1897), Whympfer (1892), Wolf (1878, 1904), and Reiss and Stübel (1869–1902). The evolution of Cotopaxi has been elucidated by Hradecka et al. (1974), Miller et al. (1978), Hall (1987), Hall and von Hillebrandt (1988), and Mothes (1992).

Eruptive activity at Cotopaxi started with the formation of an ancient stratovolcano (Paleocotopaxi, 560 ka) that was characterized by large explosive events and deposition of rhyolitic Plinian falls and ash flows (Dense Rock Equivalent [DRE] volume ~ 9.6 km 3 ; Barrancas rhyolite series in Hall and Mothes, 2008). This period culminated with the emplacement of the Murco Peak subvolcanic body (Sauer, 1965; Barberi et al., 1995; Hall, 1977, 2004a; Hall and Mothes, 2008). After the deposition of the Chalupas ignimbrite, which erupted at 211 ka from the neighboring Chalupas caldera, activity at Cotopaxi resumed 100–150 k.y. ago (Barberi et al., 1995; Hall, 1977, 2004; Hall and Mothes, 2008) with large rhyolitic Plinian eruptions and andesitic lava emissions (DRE volume ~ 6.2 km 3 ; F series in Hall and Mothes, 2008). A huge flank failure occurred ca. 4500 yr B.P. (Barberi et al., 1995; Hall, 1977, 2004; Hall and Mothes, 2008; Smyth and Clapperton, 1986), forming a dry debris avalanche in the Rfo Pita channel (Fig. 1). Hummocky topography is the only remaining evidence of the event, since the scar has been completely filled by younger eruptive products. Hall (1987) grouped Cotopaxi activity into seven main periods and 20 subunits

following Hradecka et al. (1974). Hall et al. (2004a), Hall and Mothes (2008), and Mothes (2006) further simplified the stratigraphic history of the volcano with a division into three main groups.

(1) Cotopaxi I started around 560 ka with rhyolitic-andesitic magmatism (obsidian dikes, domes, lava flows, ash, and tephra falls). The sequence lies unconformably upon a thick detrital package at the base of the Inter-Andean Valley. During the subsequent period of repose (ca. 400–13 ka), the large Chalupas ash flow (200 ka) was deposited in the area.

(2) Cotopaxi II occurred from 13,200 yr B.P. to 4100 yr B.P. Cotopaxi experienced six important rhyolitic cycles that culminated with a major flank collapse. This period of activity consisted of tephra falls, dome collapses, phreatomagmatic activity, and huge lahars. Andesitic activity was subordinate.

(3) The present andesitic eruptive history began ca. 4000 yr B.P. with tens of eruptions characterized by scoria and pumice falls, lava flows, and pyroclastic flows, all of which have contributed to the present edifice. Minor rhyolitic eruptive episodes may have occurred around 2100 yr B.P.

HISTORICAL ACTIVITY

Historical chronicles and reports concerning Cotopaxi activity are available starting from the time of the Spanish conquest. Summaries of the historical activity have been compiled by Hantke and Parodi (1966), Hradecka et al. (1974), Hall (1977), Simkin et al. (1981), and Barberi et al. (1995). In addition to published papers, we analyzed information contained in documents recovered by one of us (Aguilera) from archives of Latacunga (Cedulario de Latacunga). Here, we critically scrutinize all of the historical information and cross-check it with deposit features to assess the actual age of each tephra unit. Through this cross-checking of information between the historical chronicles and the field work, we were able to constrain, unequivocally, deposits of eruptions that occurred in 1534, 1742, 1744, 1766, 1768, 1803, 1853, 1877, and 1880. The age attribution for these events (and, in particular, from 1742 to 1880) is reliable because descriptions in the chronicles contain detailed information about the tephra dispersal and associated scoria flows and lahars. All detailed information is summarized in Table 1, and locations in the text are indicated in the map of Figure 1.

Other unconfirmed events are reported in the chronicles, but with information that is often scarce or incomplete. In these cases (1757–1758, 1857, 1866, 1885, 1903–1904, 1906,

1912, 1942), we could not unequivocally identify the counterpart deposits in the field.

Problems arise in some cases with the interpretation of the terminology used by the chroniclers. The main discrepancy is with the term “*lava liquescente*,” often translated as “lava flow”; in this work, we believe that past authors have used it in a broader sense, i.e., including any type of flowing incandescent material, regardless of its state of aggregation. The same interpretation was also made by Barberi et al. (1995) and Hall and Mothes (2008). The term *ash* (as a translation of the term *ceniza* used in the historical chronicles) indicates fine-grained tephra particles, usually less than 2 mm in diameter, although the chronicles use the term *ceniza* irrespective of any grain-size connotation.

The oldest historical account of an eruption is that of 1534 (Wolf, 1904). Agustín de Zárate (1555) reported substantial ice melting and lahar generation during the event and stated that

a village called “la Contiega” was flooded and buried; it was not possible to identify the exact location of the site, although this remains the first historical chronicle about a human settlement destroyed by a lahar in Ecuador.

More than 200 yr of inactivity, or a period with no information, followed the 1534 eruption. Cotopaxi apparently resumed its activity in 1742, when “incandescent flows” and lahars are recorded (Latacunga archives in Sodiro, 1877; Wolf, 1904). Activity continued and escalated again in November 1744, with intense ash fall reaching a thickness of 10 cm in La Cienega, near Tanicuchi, 22 km SW of the crater (Fig. 1). Generation of lava flows in different directions caused snow melting and formation of lahars that proved more destructive than the 1742 and 1743 events (Cedulario de Latacunga; La Condamine [1751] in Wolf, 1904; Parédez, 1982). As a result of the early 1740s eruptions, a letter of 1802 by the mayor of Latacunga to Alexander

von Humboldt (1804) described a general state of famine in the Latacunga Valley in the second half of the eighteenth century.

Eruptive activity resumed in 1766, after 22 yr of quiescence, with an explosive event on 10 February 1766; ash covered fields and caused roofs to collapse (Sodiro, 1877). Velasco (*in* Wolf, 1904) reported that fall out of coarse pumice on the western part of the edifice destroyed several farms. Lahars affected the town of Latacunga (Fig. 1), and the volcano remained active for the entire year.

A second and more powerful event occurred on 4 April 1768, with ash fall reaching Pasto (250 km NE, Fig. 1). Bombs fell on La Cienega (22 km SW from the crater, Fig. 1) and Tanicuchi (24 km SW from the crater, Fig. 1), causing collapse of the church roof. Burning huts and haylofts in Mulalò (15 km SW, Fig. 1) were responsible for eight casualties. Big lahars, even more powerful than the 1766 flows, were generated

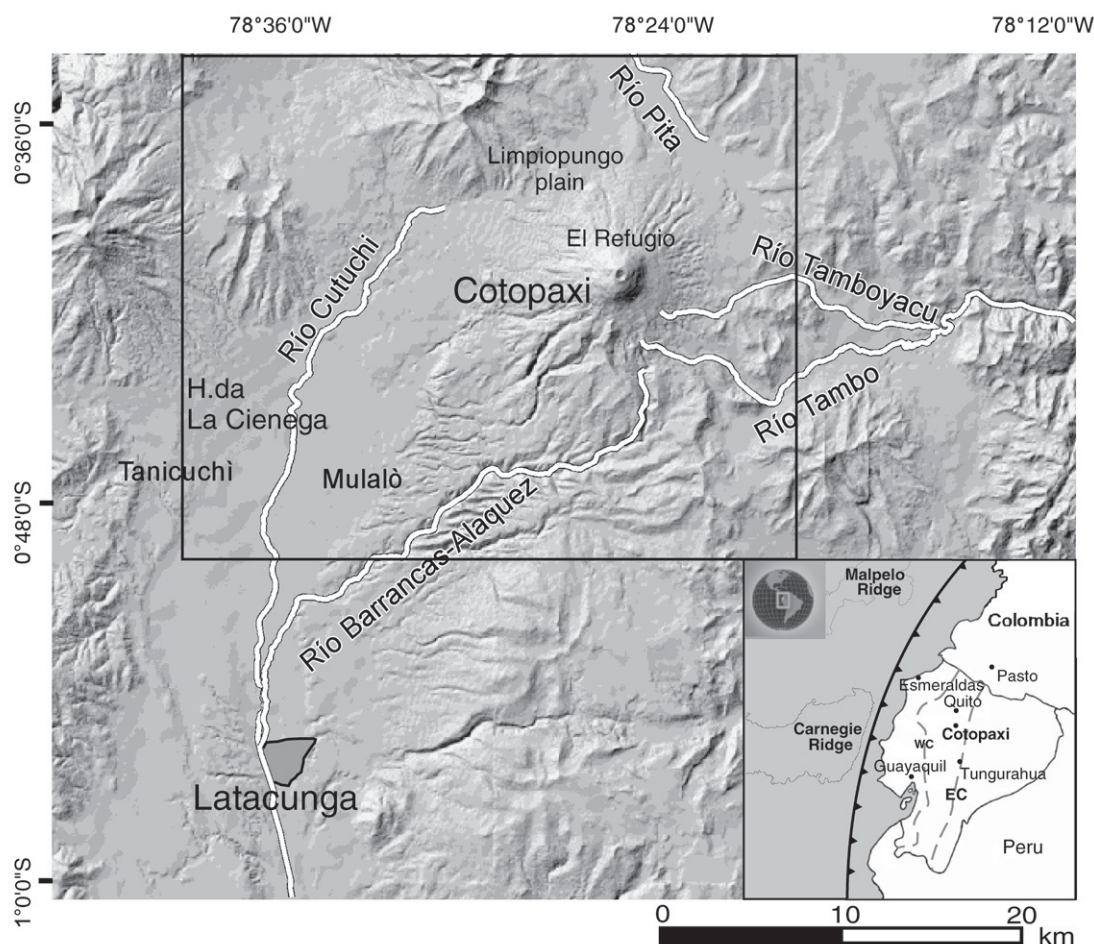


Figure 1. Shaded relief map of Cotopaxi volcano and surrounding areas with main drainage systems and locations indicated in the text and in Table 1. Black box corresponds to the area represented in Figure 2. In the inset on the bottom right, the general map shows also the main oceanic features and the trench (toothed line). WC and EC refer to Western and Eastern Cordilleras, respectively.

TABLE 1. HISTORICAL CHRONICLES AND REPORTS CONCERNING COTOPAXI ACTIVITY FROM THE TIME OF THE SPANISH CONQUEST

Date	Description	Source
1534	Ash fall that lasted for several days. Ice melting and generation of lahars. P. de Alvarado reported ash fall from Cotopaxi during his trip toward Quito. A village called "La Contiega" was flooded and buried ("hundido y anegado").	1; 2; 3; 4; 5; 6; 23
19 June 1742	Ash and gas emissions seen from Guagua Pichincha by Bouguer and La Condamine. Long ash emissions and continuous noises were the precursors of the major event. Lahars also reported. Big lahar reported in Latacunga on 24 June. No information available regarding the northern sector.	1; 7; 8; 9; 16
9 December 1742	New lahar in Latacunga, bigger than the previous of June 1742. The small village of Rumpimamba was destroyed. The "Barrio Abregado" a neighborhood of Latacunga, situated in the lower part of the city, was flooded.	17; 27
April 1743	(...) a huge amount of water came down from the cone (...) before the eruption the volcano seemed in fire, throwing flames in the sky at a height of more than 900 m (...)	8; 16
27 September 1743	Ch. La Condamine was in France but took interest in the volcanic activity of Cotopaxi.	1; 2
30 November– 2 December 1744	Eruption with intense ash fallout. Deposit thickness of 10 cm in La Cienega, near Tanicuchi, 22 km SW from the crater. W-SW dispersion. Scoria flows with snow melting and formation of lahars greater than the 1742 and the 1743 lahars.	1; 7; 8; 9; 17; 18; 27
1745	Big lahars in Latacunga; floods reached Plaza Mayor. Ice blocks were noticed in the lahar deposits. Ash fallout caused darkness in Latacunga. At midnight, 6 h after the eruption, Rio Napo overflowed. Napo inhabitants were dragged away.	19
1757–1758	M. Cicala, arriving in Quito, described the bridge on Rio Guayllabamba, north of Tumbaco, as one of the bridges destroyed in 1744 during the eruption of Cotopaxi. (...) flames over the crater were noticed up to 900 m (...)	20; 21
10 February 1766	Floods caused about 60 casualties and destroyed all the human settlements. Cotopaxi unrest motivated the temporary cessation of taxes for inhabitants.	1; 7; 8; 17; 27
April 1768	Ash covered fields and roofs until collapse. Fallout of coarse pumice on the western part caused destruction of several farms. Lahars affected the town of Latacunga, destroying the Barrio Abregado. W dispersion of the volcanic plume.	1; 7; 10; 17; 20; 23; 28
1803	Bombs fell on La Cienega, scoria fallout on Tanicuchi (24 km SW from the volcano) and Latacunga. 8 casualties in Mulaib. Deposit thickness about 30 cm in Tanicuchi. W-SW dispersion. Ash fall devastated Los Chillos valley (40 km N from the volcano) and Latacunga. Big lahars reaching Pasto (250 km NE).	7; 11; 12; 23; 22
April 1845	(...) Even in the last days of March of that year the renewed activity was noticed and intense fumarolic activity was noticed for several days. At 05:00 the volcano erupted. The explosion was heard even in the city of Popayan (...). Big lahars and a significant release of bombs, lapilli and ash. In the Valley of Pillaro roofs collapsed under the weight of ash. Total darkness throughout the day, from Quito to Latacunga. In Pedregal company, located about 16 km N-NW of the crater, ash fall caused a 53% reduction in the production of cheese. The Rio Santa Clara, near Sangoqui, was not affected by the lahar, because it did not have the volume needed to overflow the banks of the Rio Pita on the site "The Caldera" (...).	11
July–September 1853	Explosive event. Severe eruption and detonations up to 250 km, with the formation of a column of 8000 m. Lava flows, ash fallout and lahars. Explosions heard by Humboldt in Guayaquil. (...) We stopped in Guayaquil for about a month and a half, nearly witnessed the eruption that was cruel at this time the great volcano of Cotopaxi (...). Hantke and Parodi (1966) mention an eruption with a column of 8000 m in height, with detonations heard up to 250 km away, without specifying the source of these data.	1; 7; 13; 18; 23; 24
9–12 September 1854	Little information regarding the activity of this year, except for a reference by Humboldt. Abundant ash fall and emission of "lava liquescente". Ash fall is reported for 1854, but this is not confirmed. Three main lahars, destroying one of the Cutuchi bridge. Associated lava flow, composed by two streams. The eruption was observed by René de Kerret (...), the ash appeared to reach twice the height of the mountain (...). Employment of Manzanahuato lava flow, which was later described by Reiss.	18; 21
January 1855	(...) There were tremors, lapilli and ash fallout and significant floods which destroyed houses, farmlands and livestock (...). The governor of the province of Leon (now Cotopaxi) applied to the central government in the following terms: "I take the opportunity of the first light to speak ... that from twelve o'clock to one in the morning, the river Cutuchi produced tremendous noise, and was subsequently swelled to a considerable elevation; of the four arches of masonry that formed the bridge Cutuchi, the three roots are gone, leaving intact the main and larger. The current has been lowered so far more than half, however runs noisily and abundant ... that stones caught in the creek, could barely keep them in his hand still burning despite having been in long-distance water (...)	18
16–21 September 1866	(...) Cotopaxi continued throwing fire and flames and generating floods (...). (...) very dense smoke in an enlightened column. A flow of Cotopaxi destroyed the bridge Alaques, and we had to make a lengthy way to cross the river, whose shores were covered of burning sand and hot scoria and hot scoria and some semi-steaming (...)	16
1877	According to Stübel, small lava flows were emitted. (...) Liquid lava, noise, floods of Cutuchi and other demonstrations, remained on alert to cotopaxenses (...)	1; 18
23 August 1878	(...) From the beginning of the year, 1877 almost continuously a cloud or plume of steam and smoke into the crater of Cotopaxi was observed, stronger and thicker than it used to be displayed in tranquil times, and sometimes it lit up the night (...). On the night of 21 April was verified that the first significant eruption caused no damage, because their effects were limited to the volcanic cone. (...) On the eastern lip of the crater seemed to pour a river of fire (...).	1; 7
1880	On 26 June at 10 a.m. the paroxysmal eruption occurred with the emission of pyroclastic flows such as "boiling over," which melted the glaciers and triggered large lahars that traveled through all the natural drainage causing about 1000 victims and economic loss. The ash fall lasted several hours and was widely dispersed. In Quito, nightfall at 1:30 p.m. and there was need for artificial lighting. In Guayaquil the ash fall began on June 26 at nine in the morning and lasted, with brief interruptions, until July 1 (...). On average, the ash thickness reached 2 cm in Machachi, 6 mm in Quito, and less than 6 mm in Latacunga. On 27 and 28 June ash fall was reported along the coast en route from Guayaquil to Manta.	31
	Eruptive 12-km-high column and ash fall up to 300 km towards W. Between February and July, ash emissions occurred, with outpouring of little lava flows and lahars of small volume. At 05:40 on July 3, the volcano erupted as was observed by E. Whymper, from the summit of Chimborazo. (...) At 5:45 it began to get up a column of black ash in ink, which went straight into the air, with such prodigious speed that in less than a minute had risen to more than 20,000 feet above the crater rim (...)	14; 15

(continued)

TABLE 1. HISTORICAL CHRONICLES AND REPORTS CONCERNING COTOPAXI ACTIVITY FROM THE TIME OF THE SPANISH CONQUEST (continued)

Date	Description	Source
22 July 1885	Without any clear relation to some eruptive event, a major lahar traveled through the Río Pita and caused some damage in the Valley of the Chillos (...). Because of the flood of Río Pintag caused by the eruption of Cotopaxi on 22 of the current month, the estate of "Collegio" that I have rented cannot continue the work because the channels are completely destroyed. And second because the river has taken a different direction, leaving a considerable amount of stones (...)	29; 30
1903–1904	Small eruption with lava emission and lahars of scarce volume.	12
1906	Explosive activity concentrated in the crater area, with emission of bombs, lapilli, and coarse ash and the formation of a big column. Ash fell in Callo.	12; 25
1912	Small but frequent eruptions during February and March; major event in May with an ash column and gas emission.	12; 25
1942	Although 1904 is considered the last event of Cotopaxi, there is some information, not confirmed, of an eruptive event in February 1942, with emission of lava, after sporadic explosions occurred in 1922 and 1940.	26

Note: Locations in the text are indicated in the map of Figure 1. Citations are from: (1) T. Wolf (1878); (2) A. de Zárate (1555); (3) Pedro Cieza de Leon (1553); (4) Antonio de Herrera (1601–1615); (5) G. Fernandez de Oviedo y Valdes (1526); (6) F. Lopez de Gomara (1562); (7) L. Sodiro (1877); (8) J. Velasco (1844); (9) Ch. M. La Condamine (1751); (10) J. Diguja (1768); (11) A. von Humboldt (1804); (12) Hantke and Parodi (1966); (13) W. Reiss (1874); (14) E. Whympfer (1892); (15) Hradecka et al. (1974); (16) J. Avendano (1985); (17) P. Muñoz (1996); (18) J. Kolberg (1996); (19) E. Parédez (1994); (20) M. Cicala (1994); (21) J. Coba (1929); (22) F. Gonzáles Suárez (1970); (23) N. Zúñiga (1970); (24) T. Wolf (1904); (25) F. Barriga (1973); (31) A. Martínez (1994); (26) G. Hantke (1951); (27) Cedulaario de Latacunga; (28) Archivo Nacional; Sette Haciendas (1768); (29) Archivo Arzobispal (1884–1885); and (30) El Beceiro de Hijueltas (1850).

by ice melting due to scoria-flow emplacement (rivers of lava poured from the crater, "...se derramaron del crater rios de lava incandescente...", Wolf, 1904, p. 81); these lahars devastated Los Chillos valley (a densely populated drainage of the northern sector east of Quito and 40 km from the volcano) and again Latacunga.

Cotopaxi erupted again in 1803, after 35 yr of dormancy (von Humboldt, 1837–1838). Sodiro (1877) reported an explosive event on 4 January, but with scarce detail. Hantke and Parodi (1966) and Zúñiga (1989) wrote of a severe eruption and detonations heard up to 250 km away, with the formation of a column 8000 m high. Little information is available for several minor eruptive episodes that occurred in 1843 and 1852 (Barberi et al., 1995).

Sodiro (1877) reported eruptions on 13 and 15 September 1853, with abundant ash fall and emission of "lava liquescente," which traveled as rivers of fire to the base of the cone and intercalated with three main lahars. One debris flow, described as one of the most powerful, destroyed one of the Río Cutuchi bridges. From 1855 to 1866, Cotopaxi had at least four minor eruptions with ash fallout and lava flows.

A new period of intense activity started in 1877 with a long series of precursory phenomena, such as ash fall, phreatic explosions, and seismic events. This event is by far the best known thanks to many famous paintings and to the account of L. Sodiro, a local abbot who witnessed the eruption, and to T. Wolf, a German scientist who had moved to South America years before and who assembled (in the fall of 1877) several first-hand descriptions of the event. The climactic phase started around 10 a.m. on Tuesday, May 26, with the formation of a high eruptive column that suddenly darkened the western and northwestern sector of the edifice. This explosion was followed immediately by the onset of "boiling over activity" that produced scoria flows that were described by Wolf as "...a dark foamlike cloud boiled over the rim of the crater and descended all sides of the cone, much like the boiling-over of a pot of cooking rice ..." (p. 20).

Lahars arrived less than 1 h later down the main valleys, reaching Baños (at the foot of Tungurahua, 87 km south, Fig. 1) in 8 h, and Esmeraldas, on the Pacific coast at a distance of 320 km along Río Guayllabamba, in 18 h (Almeida, 1995).

Another eruption of Cotopaxi in 1880 was observed by climbers who were ascending the volcano Chimborazo; the ash cloud reached them on the Chimborazo peak after some hours (Whympfer, 1892). Hradecka et al. (1974) reported a 12-km-high column and ash fall up to 300 km to the west from this event, although

they provided no information concerning the eruptive deposits. Hall and Mothes (2008) reported the 1880 activity as a Plinian eruption (Volcanic Explosivity Index [VEI] 2–3).

Hradecka et al. (1974) also summarized accounts of post-1880 activity. In 1885, lahars were recorded in Latacunga, although there is no clear link with eruptive activity. Small-scale explosive activity is described in 1904 and 1942. Although there is no certainty about these last eruptive events, it is clear that Cotopaxi remained in a state of high activity from the mid-eighteenth century to the end of the nineteenth century, with, apart from the major crises already described, at least one event (small eruption or ash emission) every 1–2 yr (Simkin et al., 1981).

STRATIGRAPHY OF PYROCLASTIC FALL DEPOSITS AND TERMINOLOGY

Field data collection was carried out during three different surveys in 2005, 2006, and 2007 for a total duration of ~100 d. Much of the field work was conducted by two of us (Pistolesi and Rossotti). Joint field activities involving all the authors were also conducted in 2005, 2006, and 2007.

In the stratigraphic survey, available natural and road cut sections were integrated with a large number of 50- to 70-cm-deep hand-dug pits (70%–80% of the total) at prepositioned sites. In order to obtain a well-distributed grid of stratigraphic logs, many sites were reached by hiking to high elevations on the volcano's flanks. In total, 450 sites were surveyed around the cone, from a minimum distance of 1.8 km from the crater (4820 m above sea level [asl]) to a maximum distance of 25 km from a vent to the west (3130 m asl) (Fig. 2).

At each site, a detailed stratigraphic log of tephra layers was measured and described. Identification of the tephra package was facilitated by the ubiquitous occurrence of a regional marker (the A.D. 1140 Quilotoa ash bed; Athens, 1999; Di Muro et al., 2008a; Mothes and Hall, 1999, 2008), which was taken as the lower limit of the studied sequence. To avoid data loss and optimize data compilation, all information (global positioning system [GPS] coordinates, photos, and field notes) was stored in geographic information system (GIS) format, creating a geodatabase on a digital topographic base at scale of 1:50,000 that was provided by the ESPE (Escuela Politecnica del Ejercito).

The investigated tephra sequence consists of a plane-parallel succession of fallout beds, with minor scoria-bearing pyroclastic density current deposits. Identification of the tephra units was first obtained by correlating sections from the

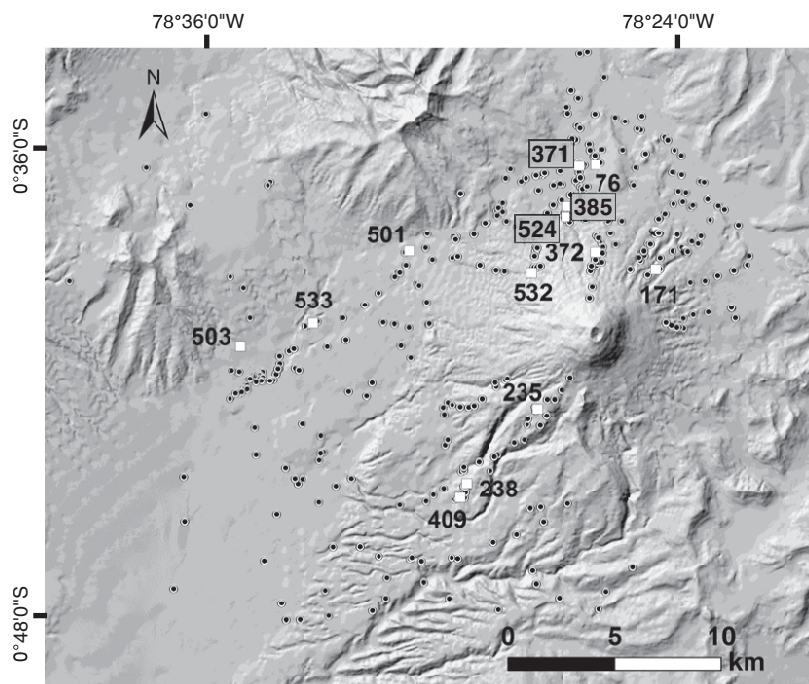


Figure 2. Shaded relief map showing the total number of sites (circles) surveyed during the field work including natural cuts and hand-dug pits. White squares show number and position of sites where sampling and detailed description of fallout layers were carried out.

interfluvial separating the main valleys within a radius of 22 km from the volcano summit. Here, the fallout sequence is well preserved, and beds can be easily correlated on the basis of lithologic features and thickness. The stratigraphic analysis was later extended to valley sites to incorporate pyroclastic flows and lahar deposits into the tephra succession.

The tephra sequence was subdivided into sets, layers, and beds based mainly on lithologic features (differences in color and grain size of deposits) and discontinuities (Fisher

and Schmincke, 1984). Tephra sets are groups of strata with similar ages that can be separated from older and younger deposits by clear evidence of elapsed time such as erosional features, soils, or reworked material. Sets can record more than one eruption; each eruptive episode represented in a set contains a series of layers and beds that can be traced as stratigraphic units, even though single beds might not be traced laterally.

Labeling of beds followed the grouping criteria suggested by Mullineaux (1996). We tried

to preserve the existing nomenclature (Barberi et al., 1995; Hall and Mothes, 2008; Mothes et al., 2004; Mothes, 2006) by modifying it only to accommodate previously unrecognized beds (Table 2). In some cases, layers described in this work were not previously recognized (e.g., layers P_R and M_V are not included in Barberi et al., 1995) or described only in the text (e.g., two fallout layers reported by Barberi et al. [1995] below layer 2, probably corresponding to layers S_W and B_L of this work). In other cases, layers have been described in detail but grouped and labeled as complex cycles (Hall and Mothes, 2008; Mothes et al., 2004; Mothes, 2006). We adopted the terminology of Hall and Mothes (2008), except that we introduced new labels for their MZ cycle. We interpret this cycle as the product of multiple eruptions, rather than a single bed set, because of the presence of soil beds associated with internal erosive unconformities.

The term *tephra fallout* is used to indicate fallout processes, whereas *tephra* is used as a collective term to describe unconsolidated, primary pyroclastic deposits (Thorarinsson, 1944). Grain sizes are described following Fisher (1961) and Schmid (1981).

Description of Tephra Units

A synthetic log of the tephra units (fallout and flow deposits) identified above the A.D. 1140 Quilotoa ash deposit and studied in this work (Fig. 3) integrates the tephra sequence observed on the northern side of the edifice (section 1 at site 372, 2°N and 3.4 km from the summit crater; Figs. 2 and 4H) with that observed on the opposite side of the cone (section 2 at site 235, 220°N and 4.1 km from the summit crater; Figs. 2 and 4B). Scoria-flow units recognized in valley sites were later inserted at their corresponding stratigraphic height by correlating fallout beds. Field descriptions of each tephra unit were integrated with representative grain-size and componentry analyses (Fig. 5; Table 3). All but two samples are from the two reference sections (sections 1 and 2); the remaining two samples are from site 533 (270°N and 13 km from the summit crater).

We identified 10 main layers above the A.D. 1140 Quilotoa ash deposit (Q), grouped in four sets. The lower sets (B and S) correspond to two tephra layers that alternate with decimeter-thick soil beds and erosive unconformities. Extensive erosion makes these tephra units laterally discontinuous. The lower set B represents a tephra deposit sandwiched between two thick soils that correspond to periods of intense erosion (stratigraphic unconformities). The overlying set S is made by a single pumice fallout layer (S_W). The upper sequence (sets M and P) consists of a plane-parallel succession of tephra layers and

TABLE 2. NEW PROPOSED LABEL SCHEME FOR LAST 1000 YR B.P. FOR COTOPAXI TEPHRA LAYERS AND CORRELATIONS OF THE SAME LAYERS WITH EARLIER WORKS

Sets	This work		Hall and Mothes (2008)	Mothes et al. (2004); Mothes (2006)	Barberi et al. (1995)
	Layers	Age			
P	P_R	Post-1880	P cycle	N cycle	1877
	P_E	1877			
	P_L	1866?			
	P_D	1853			
M	M_V	Post-1768	M cycle	M cycle	1
	M_B	1766–1768			
	M_T	1742–1744			
S	S_W	1534		MZ cycle	2
B	B_{LF}		MZ cycle		
	B_{LU}				
	B_{LL}				
	Q	1150	Y cycle	Quilotoa	QA
	X / 3		X cycle	X	3

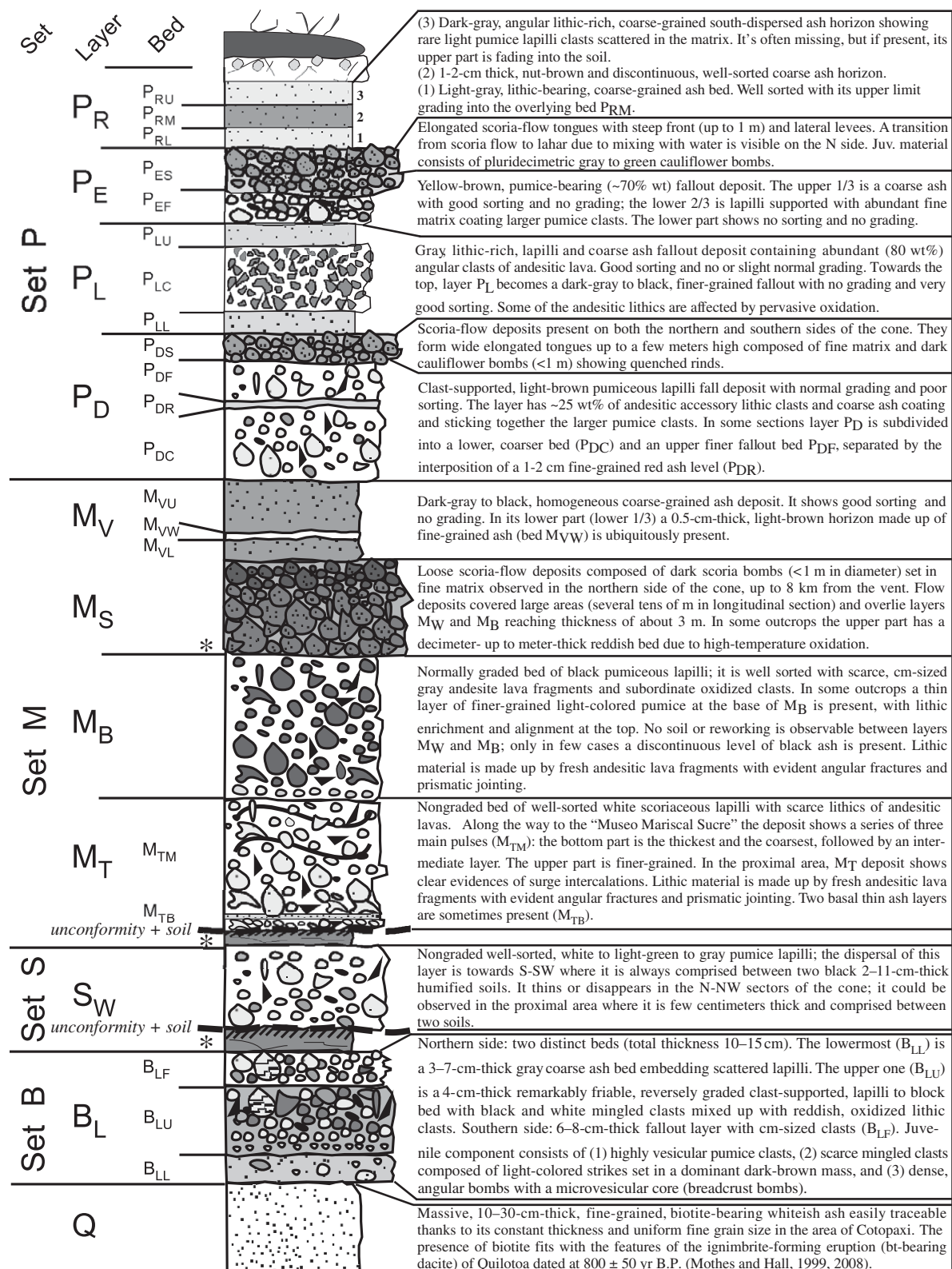


Figure 3. Reconstructed stratigraphic column of post-twelfth-century Cotopaxi eruptive history. Tephra units are described in detail in the text. The column corresponds to the tephra fallout sequence that can be observed at site 235 (Figs. 2 and 4B), although more recent layers are better exposed on the opposite side (Fig. 4H). Scoria-flow deposits are included in this stratigraphic reconstruction, but they are visible only in specific areas around the volcano. Stars refer to ¹⁴C dates on soils and charred grass.

beds with excellent lateral continuity, limited erosive unconformities, and no internal soil. The time break between set S and the overlying set M is marked by a soil and a stratigraphic erosional unconformity. Set M consists of two main

Plinian fallout events directly related to episodes of scoria-flow emplacement. The layers of the youngest set P are separated by minor erosional unconformities and deposition of reworked material. It is a complex cycle of fallout events,

scoria-flow deposits, and long-lasting period of ash emission.

Layer Q

Layer Q is dated at 810 ± 50 yr B.P. (Barberi et al., 1995; Mothes and Hall, 1999, 2008). This light-colored, biotite-bearing, fine ash deposit from Quilotoa volcano represents one of the most widespread ($>40,000$ km²) Holocene regional stratigraphic marker beds in the Northern Andes (Athens, 1999; Di Muro et al., 2008a; Mothes and Hall, 1999, 2008). The Quilotoa ash bed overlies the thickest Plinian pumice fallout deposit of the past 2000 yr of Cotopaxi activity (layer 3 in Barberi et al., 1995; layer X in Mothes et al., 2004; Mothes, 2006; and X cycle in Hall and Mothes, 2008). Layer Q can be easily identified and traced thanks to its constant thickness, uniform grain size (Fig. 4A), and ubiquitous presence of millimeter-sized biotite flakes.

Layer B_L

This layer is traceable at the scale of the whole edifice. The most proximal outcrops are well exposed on the northern side of the volcano, along the road cuts toward "El Refugio." At site 372 (3.2 km from the vent at an altitude of 4450 m; Fig. 2), the layer is made by two distinct beds, for a total thickness of 10–15 cm. The lowermost (bed B_{LU}) has a variable thickness (from 3 cm to 7 cm) and is characterized by scattered lapilli and blocks embedded within a gray, coarse ash matrix. The upper bed (B_{LU}) has constant thickness of 4 cm; it is a friable, reversely graded, clast-supported, lapilli to block bed ($Md_{\phi} = -3.36$, $\sigma_{\phi} = 1.72$) characterized by abundant black and white, spectacularly mingled, glass-bearing clasts (Fig. 4D) and oxidized lithic clasts (70–80 wt%). Decimetric ballistic blocks with well-developed radial jointing are scattered within the layer and in some cases penetrate the underlying bed or the Q layer. Late oxidation of lithic fragments caused a prominent oxidation of the whole bed. The upper bed appears to be the most widespread and can be traced around the volcano. At distances greater than 5 km from the present crater, this bed becomes a few centimeters thick and discontinuous, eventually being represented only by scattered clasts embedded in a dark soil bed.

On the southern side of the edifice (site 409), the deposit is a 6–8-cm-thick fallout deposit (B_{LS}), with centimeter-sized clasts ($Md_{\phi} = -2.60$, $\sigma_{\phi} = 2.29$) (Fig. 4B). The juvenile component (95 wt%) consists of white vesicular pumice and scattered mingled clasts similar to the northern B_{LU} bed juvenile material. B_{LS} deposit features are compatible with an episode

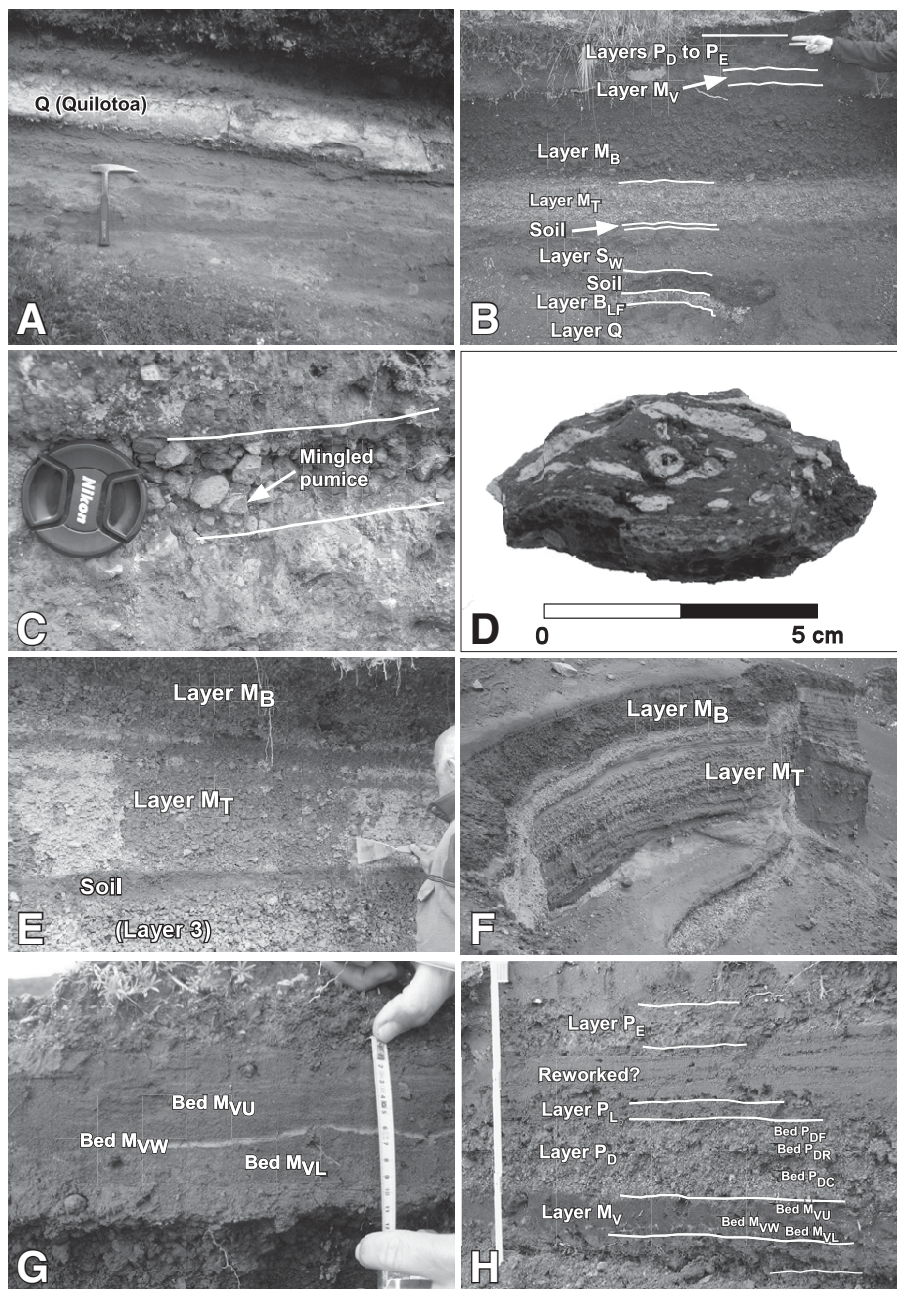


Figure 4. (A) Quilotoa white ash layer cropping out on the north flank of Cotopaxi (site 76 in Fig. 2). (B) Stratigraphic sequence from layer Q to present (fingers indicate layer P_E). The outcrop is located on the southern side of the edifice (site 409 in Fig. 2). (C) Close-up of B_L deposit: note amount of lithic material and mingled pumice (site 524 in Fig. 2). (D) Mingle pumice from layer B_L. (E) Sublayers in M_T at site 532. (F) M_T surge intercalations (80 cm in thickness) 3.7 km N-NW from the vent. (G) White ash layer M_{VW} in the lower part of layer M_V (site 238 in Fig. 2). (H) Sequence from layer M_V to layer P_E (site 372 in Fig. 2) and red ash bed P_{DR} separating bed P_{DC} from P_{DF}. Meter scale is 30 cm.

of ash venting that deposited a centimeter-thick ash layer (B_{LU}), followed by a transient, very energetic explosion (blast) that involved the disruption of lava masses (domes) and emplacement of a surge-type, highly energetic density current (B_{LU}). The fallout bed (B_{LF}) of the southern side, enriched in light pumice component, was probably related to a sustained column that formed after the disruption of the dome. The bed has been identified up to a maximum distance of

12 km from the crater. In the northern sector, a distinct, 1 cm black ash layer has been observed to directly overlie layer B_L .

Layer S_w

Layer S_w is composed of a nongraded, well-sorted, white to light-green to gray pumice lapilli bed with a maximum observed thickness of 31 cm 7 km SW of the crater. One sample collected on the southern side (site 409) yielded

$Md_\phi = -1.18$ and $\sigma_\phi = 1.85$, with a lithic content of 5 wt%.

The dispersal of this layer is toward S-SW, where it is always found between two black, centimeter-thick, humified soils. In the N-NW sector of the cone, this layer is observed only in the proximal area, where it is few centimeters thick. In the Limpiopungo plain, it is overlain by a 1–2-cm-thick black ash layer that separates it from the overlying layer M_T . Along the Pan-American Highway, 16 km W of the vent, it is represented by scattered lapilli embedded in a fine-grained soil. In total, we recognized layer S_w at 16 sites (with thickness ranging between 2 cm and 31 cm), and we interpreted it as a fall-out deposit.

Layers M_T and M_B

Layers M_T and M_B (guide horizons) form a pair of black and white tephra layers easily traceable all around the volcano. The two beds coincide with layers 2 and 1 in Barberi et al. (1995), and layers M_T and M_B in Hall and Mothes (2008), Mothes et al. (2004), and Mothes (2006). They were probably erupted in a close time interval because no intervening soil was observed (Barberi et al., 1995; Mothes et al., 2004). However, layers M_T and M_B have a slightly different dispersion, suggesting a different timing of eruption and/or a different column height. The presence of a time break is confirmed by the occurrence of interlayered stream sediments and debris-flow deposits at valley sites, and also by the sporadic occurrence of small pockets of organic material at the base of M_B .

Samples of layers M_T and M_B were collected on the western slope, 13 km from the crater (site 533). At this locality, layer M_T is a nongraded bed of well-sorted white to tan scoriaceous lapilli ($\sigma_\phi = 1.55$, $Md_\phi = -1.35$) with scarce lithic fragments (4 wt%) of andesitic lavas and very subordinate loose crystals (0.2 wt%). In the same locality, M_B is a normally graded bed of black scoria lapilli ($Md_\phi = -1.47$); it is well sorted ($\sigma_\phi = 1.93$) with scarce, centimeter-sized gray andesite lava fragments and minor oxidized clasts (4 wt%), and very subordinate loose crystals (0.2 wt%).

Layer M_T was identified in more than 80 sites, with a maximum observed thickness of 80 cm, ~8.4 km W of the crater. Along the way to the Limpiopungo plain (Fig. 1), the deposit, up to 1 m thick, consists of three lapilli beds (M_{TM}) separated by centimeter-thick ash beds. The bottom bed is the thickest and the coarsest, and it is followed by a central layer of intermediate grain size (Fig. 4E); the upper subbed is the finest grained. In this same locality, M_T overlies two ash beds, 3 and 5 cm thick (M_{TB}), that record the

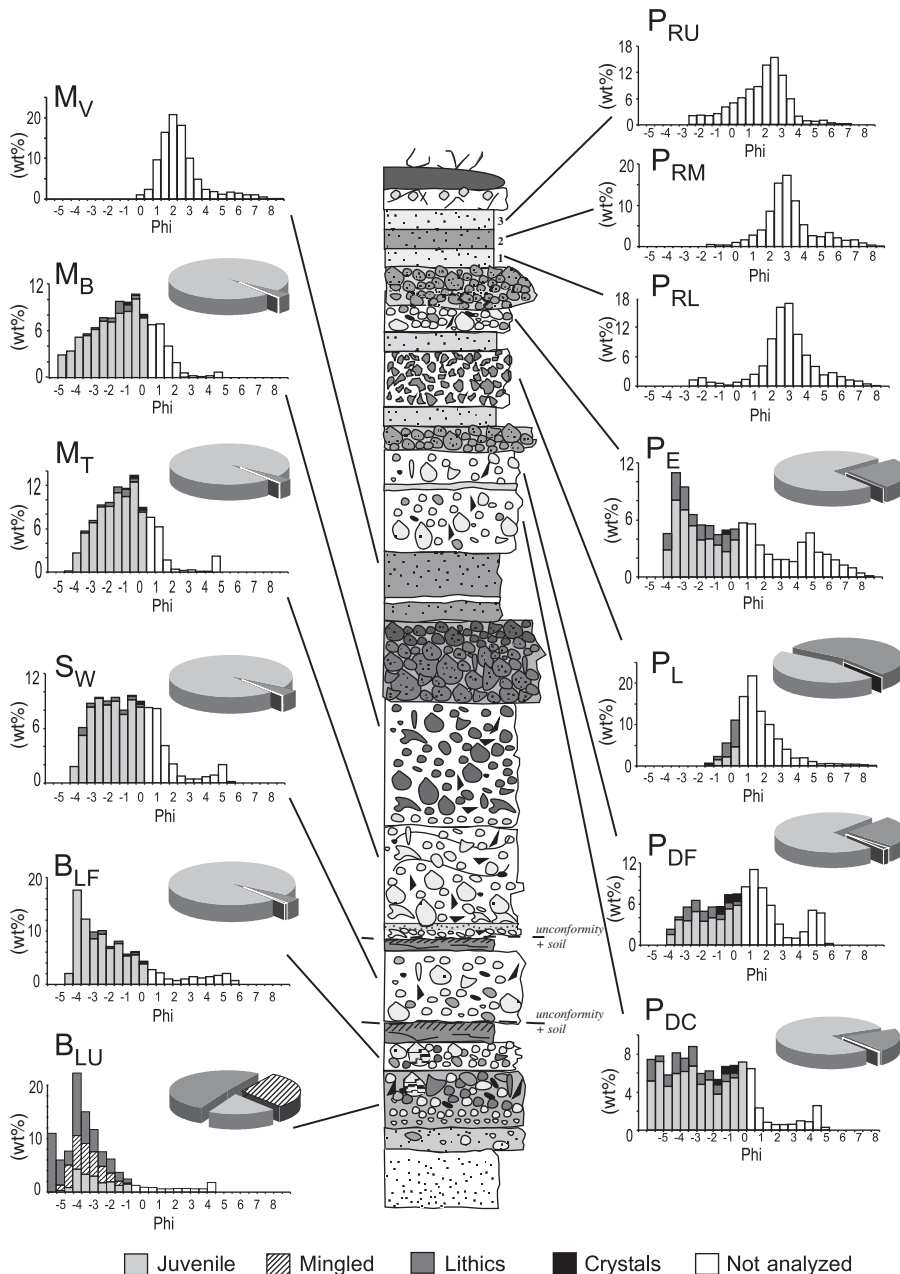


Figure 5. Grain-size and componentry histograms of fall deposits. Dark-gray boxes indicate the accidental lithic component, gray and black boxes indicate juvenile and loose crystals components, respectively, and dashed boxes represent mingled clasts. Pie diagrams show the relative abundance of the four components.

TABLE 3. DETAILS OF GRAIN-SIZE DATA OF PROCESSED SAMPLES, SAMPLING SITES, AND DISTANCES FROM THE VENT

Sample	Layer	Sampling site	Distance (km)	Md ϕ	$\sigma\phi$	K ϕ	% sample processed	% juvenile	% lithics	% crystals	% mingled
CX 34	P _{RIU}	235	4.1	1.69	1.60	0.95	—	—	—	—	—
CX 35	P _{RM}	235	4.1	2.70	1.51	1.09	—	—	—	—	—
CX 36	P _{RL}	235	4.1	2.13	1.62	1.35	—	—	—	—	—
CX 37	P _{EF}	372	3.4	-0.70	3.42	0.63	57.1	75.3	24.4	0.3	—
CX 30	P _L	235	4.1	0.82	1.47	0.98	19.3	44.9	55.1	0.0	—
CX 59	P _{DF}	372	3.4	2.13	2.51	0.74	49.3	72.8	25.2	2.0	—
CX 58	P _{DC}	372	3.4	0.04	2.53	0.64	76.7	79.4	20.1	0.4	—
CX 32	M _{VU}	235	4.1	2.43	1.03	0.83	—	—	—	—	—
CX 45	M _B	533	13	-1.47	1.93	0.77	78.1	95.9	3.9	0.2	—
CX 46	M _T	533	13	-1.35	1.55	0.75	80.6	95.8	4.0	0.2	—
CX 63	S _W	409	9.6	-1.18	1.85	0.66	71.7	94.7	5.1	0.2	—
CX 64	B _{LF}	409	9.6	-2.60	2.29	0.63	83.6	95.1	4.2	0.7	—
CX 507	B _{LU}	372	3.4	-3.36	1.45	0.66	91.71	18.5	51.3	0.0	30.1

Note: Median diameter (Md ϕ), standard deviation ($\sigma\phi$), and kurtosis (K ϕ) parameters are from Inman (1952) and Folk and Ward (1957).

low-energy explosive activity that heralded the main M_T event. We interpreted the M_T deposit as related to a Plinian fallout: In the proximal area, 3.7 km N-NW from the vent, the deposit shows clear evidence of surge intercalations possibly related to collapsing phases of the Plinian column (Fig. 4F).

Layer M_B was examined in more than 100 sites; the maximum observed thickness is 70 cm, 6.3 km SW from the crater. In several outcrops, the base of layer M_B is characterized by the presence of light-colored microvesicular pumice and minor fresh, angular fragments of light-gray lava. Lithic material of M_T layers consists of fresh, light-gray, variably vesicular, andesitic lava fragments with radial prismatic jointing, possibly deriving from the disruption of a still-hot lava dome mass.

Loose, coarse-grained tephra deposits (layer M_S) composed of dark, cauliflower scoria bombs (1 m in diameter) set in a fine-grained matrix are interlayered in the upper part of M_B on the northern side of the cone, up to 8 km from the vent. The deposits consist of multiple tongues that are several meters wide and up to 3 m thick. The upper part of the units is commonly oxidized and may show a rough columnar jointing suggestive of high-temperature emplacement (Fig. 6A). Most of the units are rich in juvenile bombs, although some others have abundant exotic lithic clasts of altered lavas that were likely derived from the volcanic conduit walls. Some of these deposits were interpreted by Hall and Mothes (2008) as lahar deposits. However, we interpret the same deposits as scoria flows emplaced at high temperature on the basis of their incipient welding and extensive oxidation of the juvenile scoriae. Layer M_B is present both at the base and at the top (3–4-cm-thick bed) of the scoria-flow deposit, suggesting that scoria-flow units were emplaced during the fallout phase, but after its climax.

Layer M_V

Layer M_V is a dark gray to black, massive, coarse ash deposit. In section 2, it shows Md ϕ = 2.43, good sorting ($\sigma\phi$ = 1.03), and no grading. We examined layer M_V in more than 200 sites. The maximum observed thickness is ~30 cm, 9.5 km W-NW of the crater. The upper boundary with the overlying layer P_D is sharp. In its lower third, a 0.5-cm-thick, light-brown horizon (Fig. 4G) made up of fine-grained ash (bed M_{VW}) is ubiquitously present. Both the thickness and grain size of this horizon are nearly invariant at the scale of the volcano, making the bed a characteristic guide horizon. We interpret layer

M_V as an ash fallout deposit from a moderate, long-lasting explosive activity.

Layer P_D

Layer P_D is a clast-supported deposit of light-brown, pumice lapilli. In section 1, it has Md ϕ = -2.13, with slight normal grading and poor sorting ($\sigma\phi$ = 2.51). The contact with layer P_L is sharp (Fig. 4H). In section 1, it was possible to subdivide layer P_D into two beds: the lower bed (P_{DC}) is overlain by a finer-grained fallout bed (P_{DR}) ($\sigma\phi$ = 2.53, Md ϕ = 0.04). The two beds are separated by the interposition of a 1–2 cm fine-grained red ash level (P_{DR}). The cumulative

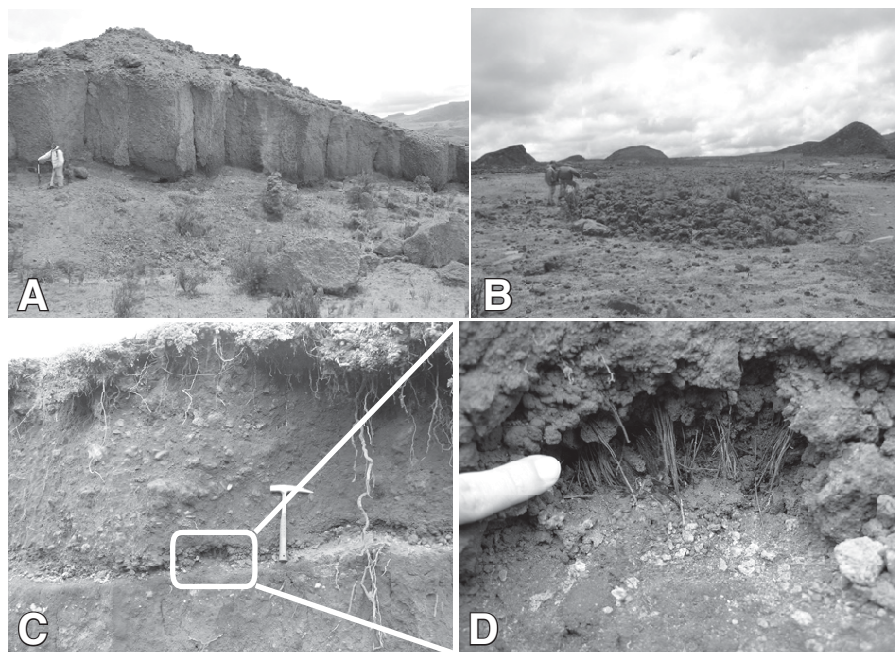


Figure 6. (A) M_S welded scoria flow with its reddish upper zone in the northern sector. (B) P_{ES} scoria-flow tongue of the eastern sector (hummocks in the background). (C) Burned grass found at the base of layer M_S. (D) Close-up of white box in C.

thickness of beds P_{DC} and P_{DF} was measured in more than 170 sites; the maximum thickness is ~25 cm, 5.7 km N of the crater. The dispersal of this layer, here interpreted as a fallout deposit, is to the west.

Associated loose scoria deposits (P_{DS}) are present on both the northern and southern sides of the cone. They form elongated tongues up to a few meters thick formed by dark cauliflower bombs (<1 m) in a fine-grained matrix. The bombs bear glassy rinds, possibly formed by quenching during interaction with the summit glacier. We interpreted these deposits as scoria flows related to boiling-over activity; they are present at the top of layer P_D , and, at some sites, are interlayered between beds P_{DC} and P_{DF} . Bed P_{DR} could correspond to the ash deposit related to scoria-flow emplacement.

Layer P_L

Layer P_L is a gray, lithic-rich, lapilli and coarse ash deposit containing abundant angular clasts of lithic and dense juvenile material. In section 2, the layer exhibits $Md_\phi = 0.82$, good sorting ($\sigma_\phi = 1.47$), and faint normal grading (Fig. 4H). Toward the top, layer P_L becomes a dark-gray to black, fine-grained ash deposit with no grading and very good sorting. In the southern sector, it is formed by three distinct beds. Component analysis yields over 80 wt% of dense andesitic, variably vesicular clasts and only ~20 wt% of pumice (bed P_{LC}). Some of the lithic clasts are affected by pervasive oxidation. We observed and measured layer P_L at 170 sites. The main dispersal of this layer is toward the W-SW, reaching a maximum thickness of 13 cm at 2.8 km S of the vent. In the northern sector, it forms a 1–2 cm bed of gray ash. Where layer P_L is thicker, it contains a basal dark-gray, lithic-bearing, ash horizon with rare fine pumice clasts (bed P_{LL}), and, at the top, 2 cm of ash (bed P_{LU}). We interpret layer P_L as a fallout deposit.

Layer P_E

Layer P_E is a yellow-brown, pumice-bearing (~70 wt%) deposit (Fig. 4H). In section 1, the deposit has $Md_\phi = -0.70$ and $\sigma_\phi = 3.42$. Layer P_E was measured in ~200 sites and has a maximum observed thickness of 15 cm, 4.2 km N of the crater, along the road to the refuge. The dispersal of this layer suggests that it is a fallout deposit directed to the north-northwestern sector of the volcano.

Associated loose scoria deposits (P_{ES}) are visible in the northern and northeastern parts of the cone. They form elongated tongues with steep fronts up to 1 m high and lateral levees a few decimeters high (Fig. 6B). Juvenile material consists of up to 80-cm-diameter, gray to green cauliflower to breadcrusted bombs concentrated

in the outer part of the flow. The inner part of the unit is rich in fine matrix engulfing decimetric juvenile bombs and lithic fragments of older lavas. We related P_{ES} to scoria-flow deposit related to boiling-over activity.

Layer P_R

Layer P_R is formed by three main beds and represents the top part of the succession.

Bed P_{RL}

Bed P_{RL} is a light-gray, lithic-bearing, coarse-grained ash bed. In section 2, it has $Md_\phi = 2.13$. It is well sorted ($\sigma_\phi = 1.62$), and its upper limit grades into the overlying bed P_{RM} . It is dispersed to the south, reaching 1–2 cm at 4.1 km SW of the crater.

Bed P_{RM}

Bed P_{RM} is a 1–2-cm-thick, nut-brown and discontinuous, well-sorted coarse ash horizon ($\sigma_\phi = 1.51$, $Md_\phi = 2.70$, section 2).

Bed P_{RU}

Bed P_{RU} is a dark-gray, angular lithic-rich, coarse-grained ($Md_\phi = 1.69$) ash horizon showing rare light pumice lapilli clasts scattered in the matrix. This layer is commonly missing, but if present, its upper part fades into the soil. It shows good sorting ($\sigma_\phi = 1.60$, section 2) and is south-dispersed (3 cm thick at 4.1 km south of the vent). All P_R layers are limited to the southern part of the cone and are preserved only in proximal areas. They are interpreted as ash fallout deposits.

TEPHRA AGE ATTRIBUTION

Assignment of tephra units to specific historical eruption episodes was made by:

(1) constraining tephra age through four new radiocarbon dates on selected carbon-rich soils samples and charred grass; and

(2) matching field characteristics of deposits with historical descriptions of eruptive phenomena and their effects (eruptive sequences, tephra dispersion, material size, and deposit thickness).

Our interpretation of the ^{14}C dates assumes that the historical chronicles cover the entire period from the Spanish Conquest to present, without missing any significant eruptive event; this assumption is supported by the correspondence between the number of tephra deposits that we found in the field and major eruptive crises described in the historical accounts.

Two ^{14}C Accelerator Mass Spectrometry (AMS) analyses were performed on soil samples collected from a stratigraphic section 7.9 km south from the crater (site 409). CX-501 represents the topmost part of the soil bed between layers S_W and

M_T (immediately underlying M_T). CX-502 represents the topmost part of the soil between layers B_L and S_W (immediately underlying S_W).

Sample CX-502 yielded a 2σ calibrated age ranging from A.D. 1480 to 1660 (95% probability), and corresponding to 1σ time windows of A.D. 1520–1580 and A.D. 1630–1650. Because the seventeenth-century age falls within a period with no reported activity, we assume that the age of the bed is consistent with that of A.D. 1534 eruption. The southern dispersion of S_W tephra is in agreement with historical accounts. The eruption may correspond to the one reported by the Spaniards Sebastian de Béalcazar and Pedro de Alvarado, who were conquering the highlands of Ecuador in A.D. 1534 (Mothes et al., 2004). The presence of a soil between the Quilotoa ash and layer B_L suggests a prolonged period of volcanic quiescence at Cotopaxi between these events. Layer B_L should thus correspond to a single event that occurred between the Quilotoa eruption (A.D. 1140) and the formation of the soil dated between A.D. 1480 and 1660.

The CX-501 radiocarbon age also intercepts the calibration curve at several places: 1σ intervals are consistent with three time windows at A.D. 1660–1680, 1740–1810, and 1930–1950 (Table 4). By excluding the oldest age, because the volcano was not recognized as active and the youngest one because it is too recent, the remaining time window makes layer M_T consistent with the eighteenth-century eruptions.

Two ^{14}C dates were obtained from charred grass at the base of scoria-flow M_S (Figs. 6C and 6D). Samples (CXSV-1 and CXSR-1) were collected in the same stratigraphic position at two different sites at 7.6 and 5.8 km north of the crater (sites 371 and 385, respectively; Fig. 2).

AMS results for CXSV-1 gave three possible time windows: A.D. 1640 to 1680, A.D. 1730 to 1810, and A.D. 1930 to 1950 (Table 4). Using the same rationale adopted for CX-501, we consider the A.D. 1730–1810 time window as the most probable. Standard radiocarbon methods used on CXSR-1 yielded a slightly broader 2σ radiocarbon age (A.D. 1640 to 1950). Since the radiocarbon age intercepts the calibration curve at several points, we obtained again three time intervals (A.D. 1660–1690, 1730–1810, and 1920–1950) for the 1σ interval (Table 4). Again, we consider A.D. 1730 to 1810 as the most reliable date. Using these bracketing ages, and considering that scoria-flow M_S was emplaced during the M_B eruption, we conclude that the M_T , M_B , and M_S units likely correspond to the two major eruptive crises described in historical chronicles during the eighteenth century (A.D. 1742–1744 and A.D. 1766–1768, respectively).

TABLE 4. RESULTS OF RADIOCARBON AGE DETERMINATIONS AND CALENDAR AGE CONVERSION (68% AND 95% PROBABILITIES) ANALYSES, SAMPLING LOCATIONS (SEE FIGURE 2), AND SAMPLE STRATIGRAPHIC HEIGHTS

Sample	Type of sample	Method	Sampling site	Stratigraphic height	^{14}C yr B.P. ($\pm 1\sigma$)	$^{12}\text{C}/^{13}\text{C}$ (‰)	Calendar age A.D. (1 σ , 68%)	Calendar age A.D. (2 σ , 95%)
CXSV-1	Charred material	AMS	371	M _s base	220 \pm 40	-23.1	1650–1670 1770–1800 1940–1950	1640–1680 1730–1810 1930–1950
CXSR-1	Charred material	Radiometric	385	M _s base	180 \pm 60	-21.9	1660–1690 1730–1810 1920–1950	1640–1680 1730–1810 1920–1950
CX 501	Organic sediment	AMS	409	S _w top	190 \pm 40	-25.3	1660–1680 1740–1810 1930–1950	1650–1700 1720–1820 1840–1880 1920–1950
CX 502	Organic sediment	AMS	409	B _L top	290 \pm 40	-21.1	1520–1580 1630–1650	1480–1660

Our association of the 1742–1744 activity with M_T matches the WNW dispersion of the fallout and is in agreement with the evidence for repeated events within a close time period. It is also consistent with the discovery of large and almost intact ceramic roof tiles in lahar deposits associated with the event (Mothes et al., 2004). Basing on the fact that Spanish built haciendas in the Latacunga Valley during the 200 yr eruptive pause from 1534 to 1742, Mothes et al. (2004) concluded that these colonial-era tiles were embedded in lahar deposits associated with the 1742 event.

There is no evidence of soil formation or important erosion/reworking between layers M_T and M_B. Mothes et al. (2004) proposed that the M_B scoria deposit was formed during the 1744 eruption. We suggest the 1766–1768 eruption as the source for this scoria layer since it corresponds more closely to the description reported in the chronicles (dispersal, size of the material; Table 1) and because all of the events younger than M_B were smaller and not capable of producing the described level of destruction. This conclusion also accords with the sporadic occurrence of organic material at the base of M_B. The fine ash layer at the base of layer M_B could record the sporadic eruptive activity described in the period between A.D. 1744 and 1766, possibly related to the growth of a lava dome. Overlying layer M_V is almost everywhere conformable on M_B, although a limited amount of reworking has been observed within this deposit at some valley sites. The sedimentological features of the layer suggest that it derives from a long-lasting ash emission, possibly preceded by a short eruptive pause (years).

Little ambiguity exists with the attribution of layer P_E to the 1877 eruption. Both the stratigraphic position and the dispersal of the layer are consistent with historical descriptions. Scoria-flow deposits and lahar generation observed in the field match the timing and geographic distribution of products given by Wolf (1878) and Sodiro (1877) for this eruption.

Using this general architecture of layers with a clearly identified age, we can insert the remaining layers using deposit features and historical accounts. On the basis of sedimentological features, bed M_{VW}, embedded in M_V, is interpreted as a distal ash fall from a different volcano. A reasonable source eruption of this bed could be a 1773 eruption of Tungurahua volcano (Fig. 1). Excellent preservation of this thin (mm) uniform fine ash bed within M_V at all sites suggests that the distal ash represents a short-lived ash-fall event that was deposited during a period of frequent ash emission of Cotopaxi and promptly buried.

Layer P_D shows features that fit descriptions of the 1853 activity. A time lapse between M_V and P_D is marked by the occurrence of reworked sediments. The description of abundant ash fall and emission of “*lava liquesciente*” reported by the chronicles for the events of 1853 accords well with our findings of scoria-flow deposits (unit P_{DS}) at the top of the P_D sequence. The deposit of Quebrada Manzanahuaico (western side of the cone), which is described by Reiss (1874) and Wolf (1878) as a lava flow, has been identified in the field and interpreted as a scoria-flow deposit (Hall and Mothes, 2008). The age of P_L is ambiguous. It could correspond to the 1866 eruption (Barberi et al., 1995). Scoria-flow emplacement is reported in the chronicles for this event, but we could not identify the corresponding deposits in the field. Alternatively, it could be considered the starting phase of 1877 activity. Layers P_R are interpreted as all the post-1877 activity: they can represent the 1880 eruption or younger events reported in the chronicles that have limited dispersal and are confined at high elevations (Table 1).

COMPOSITION AND TEXTURE OF JUVENILE FRACTION

Petrographic Features

Petrographic observation and bulk chemical analyses were carried out on the juvenile

fraction of the main tephra beds. Petrographic features of all samples are rather monotonous: the phenocryst assemblage includes plagioclase, clinopyroxene, orthopyroxene, and magnetite. Olivine is present in most cases as an accessory mineral (layer S_w, M_T, M_B, P_E) and in reaction with clinopyroxene. Only layer B_L has amphibole (hornblende) with reaction rims. The vesicle-free porphyricity is ~20% in all cases. Variably microlitic, transparent glass and dark-yellow glass are both present in the juvenile material.

Major-Element Chemistry

Bulk chemical analyses were performed on nine samples (Table 5). Major-element values for all samples cluster in a narrow range and lie well within the spectrum of compositions erupted over the past 2000 yr (Barberi et al., 1995). All nine samples can be classified as basaltic andesite to andesite (Fig. 7A); seven of the samples are tightly clustered between 55.9 and 58.7 wt% SiO₂. Pumice from layer B_L, the oldest of the studied sequence, was analyzed after separation of the two mingled portions (Fig. 4D); SiO₂ values are 57.5 wt% and 63.3 wt%, the latter representing the most evolved composition of the entire 800 yr sequence. This sample could result from the mingling of poorly evolved magma with a magma remnant from the previous layer 3 event (A.D. 1130; 61.7 wt% SiO₂; Barberi et al., 1995).

Microscopic Textures and Glass Compositions

Major elements of the matrix glass were analyzed using a scanning electron microscope (SEM) equipped with an energy-dispersive X-ray system (EDS) at Dipartimento di Scienze della Terra of Pisa. Instrumental conditions were: accelerating voltage 20 kV; live time 100 s; counts per second ~2700; electronic beam 0.2–0.5 μm ; and beam current of

TABLE 5. INDUCTIVELY COUPLED PLASMA-MASS SPECTROMETRY (ICP-MS) ANALYSES OF MAJOR AND TRACE ELEMENTS OF COTOPAXI SAMPLES

Sample	SiO ₂ (%)	Al ₂ O ₃ (%)	Fe ₂ O ₃ (T)(%)	MnO (%)	MgO (%)	CaO (%)	Na ₂ O (%)	K ₂ O (%)	TiO ₂ (%)	P ₂ O ₅ (%)	LOI (%)	Ce (ppm)	La (ppm)	Ba (ppm)	Nb (ppm)	Zr (ppm)	Y (ppm)	Sr (ppm)	Rb (ppm)	Zn (ppm)	Co (ppm)	V (ppm)	Th (ppm)	Yb (ppm)	Dy (ppm)	Tb (ppm)	Eu (ppm)	Sm (ppm)	Nd (ppm)
CX 65 (P _{EF})	58.22	17.54	7.12	0.107	3.38	6.62	3.72	1.31	0.777	0.24	<0.01	30	14.6	5.7	5.7	106	13.6	594	29	70	18	175	3.66	1.22	2.56	0.46	1.04	3.35	15.7
CX 39 (P _{LC})	57.01	17.62	7.51	0.109	3.43	6.8	4.06	1.4	0.856	0.29	0.16	39.1	19.2	13	13	117	14.1	711	33	100	25	185	3.96	1.31	2.81	0.55	1.23	4.05	19.2
CX 59 (P _{DF})	56.3	17.46	7.44	0.108	3.59	6.94	4.08	1.39	0.886	0.3	0.03	37.8	18.6	6.2	6.2	117	12.6	715	28	80	16	184	3.76	1.19	2.71	0.52	1.24	4.06	19.2
CX 58 (P _{DC})	57.64	17.7	7.23	0.105	3.51	6.65	3.88	1.33	0.865	0.28	0.02	34.5	16.8	7.8	7.8	109	12.7	695	27	80	19	180	3.45	1.07	2.52	0.5	1.13	3.73	17.6
CX 45 (M _B)	55.93	17.47	7.9	0.118	3.83	7.1	3.91	1.2	0.87	0.28	0.4	33.7	16.2	5.8	5.8	104	13.8	681	26	90	19	185	2.96	1.25	2.7	1.18	3.82	17.8	
CX 46 (M ₁)	58.77	17.44	7.2	0.118	3.13	6.5	4.02	1.33	0.701	0.25	0.42	30.4	14.6	5.3	5.3	111	14.4	588	30	80	15	148	3.29	1.39	2.8	0.53	1.12	3.53	15.9
CX 63 (S _w)	57.2	16.96	7.57	0.118	3.97	6.91	3.85	1.29	0.783	0.24	0.14	30.6	14.3	5.6	5.6	112	14.7	585	31	80	19	175	3.44	1.32	2.76	0.52	1.14	3.62	16.1
CX 511 (B _{L1})	57.58	17.65	7.88	0.121	3.69	6.96	3.82	1.18	0.785	0.25	0.26	28.2	13.7	4.5	4.5	119	13.7	611	21	100	22	173	2.6	1.24	2.56	0.46	1.05	3.49	15.9
CX 507 (B ₂)	63.03	16.95	5.61	0.106	1.84	5.25	3.9	1.58	0.508	0.23	1.42	29.7	15	6.57	10.5	141	13.4	501	37	90	9	82	3.92	1.21	2.39	0.43	0.89	3.2	15.6

Note: B_{L1} and B_{L2} refer to bulk rock analyses of the two separated components of a mingled clast. Layers M₁ and M₂ were also analyzed by Barberi et al. (1995) (layers 1 and 2; Table 2). LOI—loss on ignition.

~1 nA. The glass compositions range from 57 to 76 wt% SiO₂. In a plot of total alkalis versus silica (Fig. 7B), analyzed glasses lie within the fields of andesite, dacite, trachyandesite, and trachydacite. There is no systematic variation in the composition of the two glass types (dark-yellow and transparent) observed in thin section (Fig. 8A). Backscattered electron (BSE) images show two different clast types: pumice-like, glassy fragments and dense, microlite-rich clasts. The first type is present in all layers and consists of highly vesicular, crystal-poor fragments with few microlites in the glass (Fig. 8C). Vesicles are typically spherical but may be highly deformed (Fig. 8D). The second type is formed by low-vesicularity, crystal-rich fragments (Fig. 8B). Vesicles, when present, are spherical. Clasts from layers P_R and M_V (ash beds erupted during long-lasting ash emission activity) belong to this category, consistent with their formation as persistent ash fall accompanying dome extrusion.

The millimeter-thick bed M_{VW} is composed of highly vesicular, microlite-free fragments, while the embedding black layer M_V is formed by dense, glassy fragments. The contrasting features of the juvenile material support conclusions from the field characteristics that M_{VW} ash is related to an exotic source.

Layer B_L contains juvenile fragments that are unusual in the context of the recent history of Cotopaxi. These clasts are characterized by convoluted blobs of white material set in a dark brown matrix (Fig. 4D). Glass analyses of the different portions of one clast indicate the presence of rhyolitic glass in dacitic pumice (68–76 wt% SiO₂), in agreement with the measured bulk composition.

ERUPTION PARAMETERS

Volumes of Fallout Layers

Compilation of isopach maps was possible for six layers (M_T, M_B, M_V, P_D, P_L, and P_E) (See GSA Data Repository). Layer P_D was mapped as a single tephra bed due to the difficulty of reliably separating beds P_{DC} and P_{DF} in the field. For layers B_L and S_w, only the dispersal area is presented, since too few points are available to construct isolines. The general trend of dispersal is elongate to the west (Fig. 9), in agreement with the direction of the prevailing winds. Isopach lines for layers M_T, M_B, P_D, P_L, and P_E were obtained by extrapolating a number of surveyed points (between 90 and 200). Layer M_V has nearly circular isopach lines, possibly the result of a long-lasting activity under variable wind directions. Additionally, although we measured thickness of M_V at more than 200 sites, we defined only

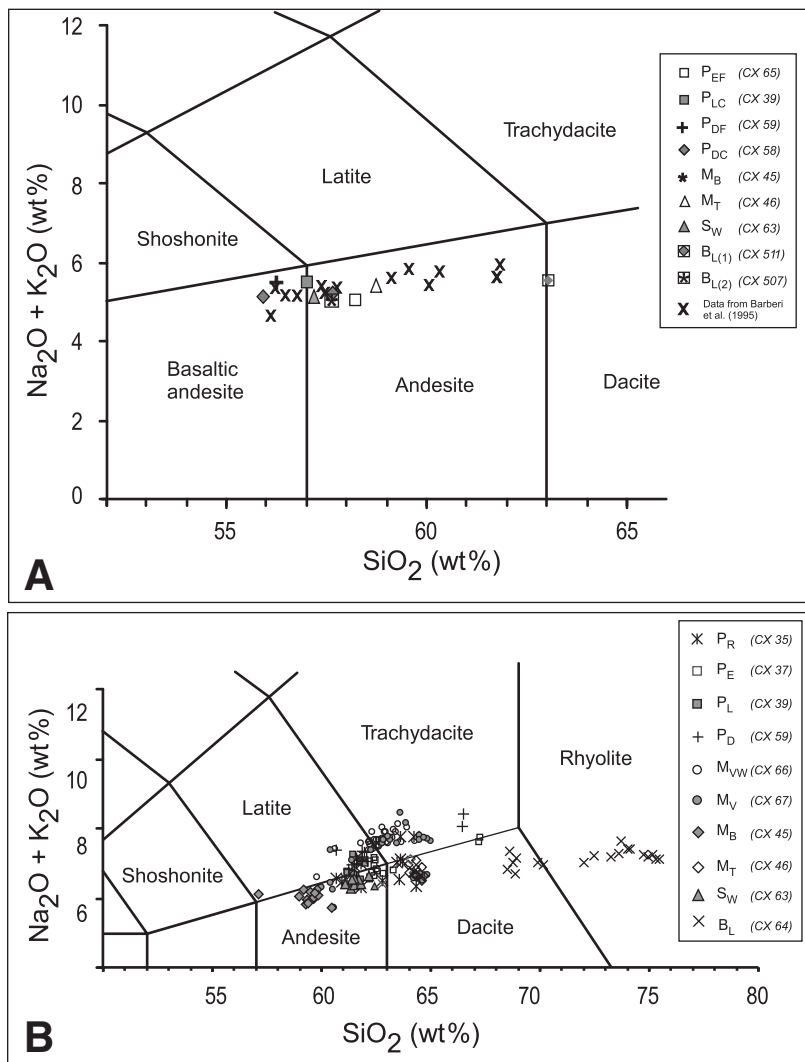


Figure 7. TAS (total alkali versus SiO_2 wt%) diagram (Le Bas et al., 1986) of Cotopaxi samples for (A) bulk compositions (data from Barberi et al. [1995] are also shown for comparison) and (B) scanning-electron microscope–energy dispersive spectrometry (SEM-EDS) analyzed glass compositions. $B_{L(1)}$ and $B_{L(2)}$ refer to bulk rock analyses of the two separated components of a mingled clast.

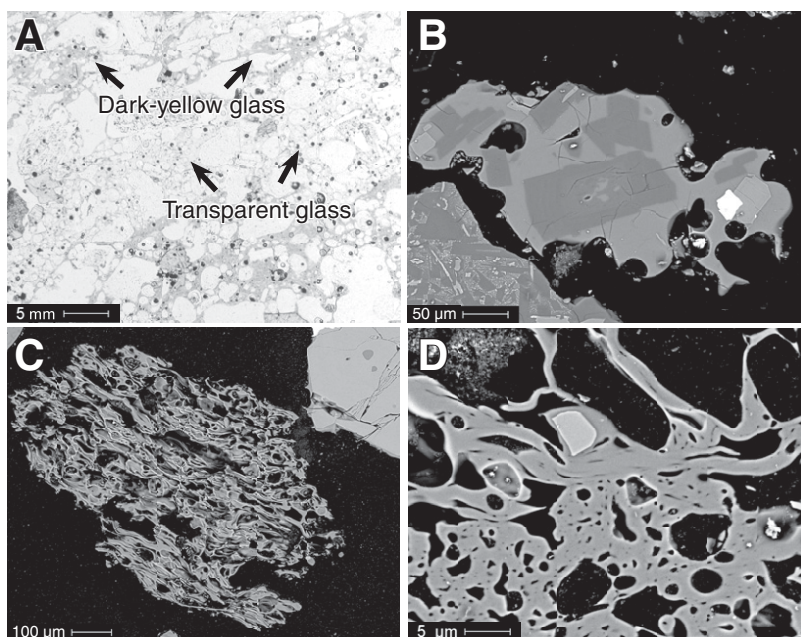


Figure 8. (A) Photomicrograph of glass in a banded clast of sample CX 44 (layer P_{ES}). Backscattered images of tephra fragments: (B) low-vesicularity clast of sample CX 35 (layer P_{RM}); (C) highly vesicular fragment in sample CX 59 (layer P_{DF}); and (D) stretched bubbles in sample CX 46 (layer M_T).

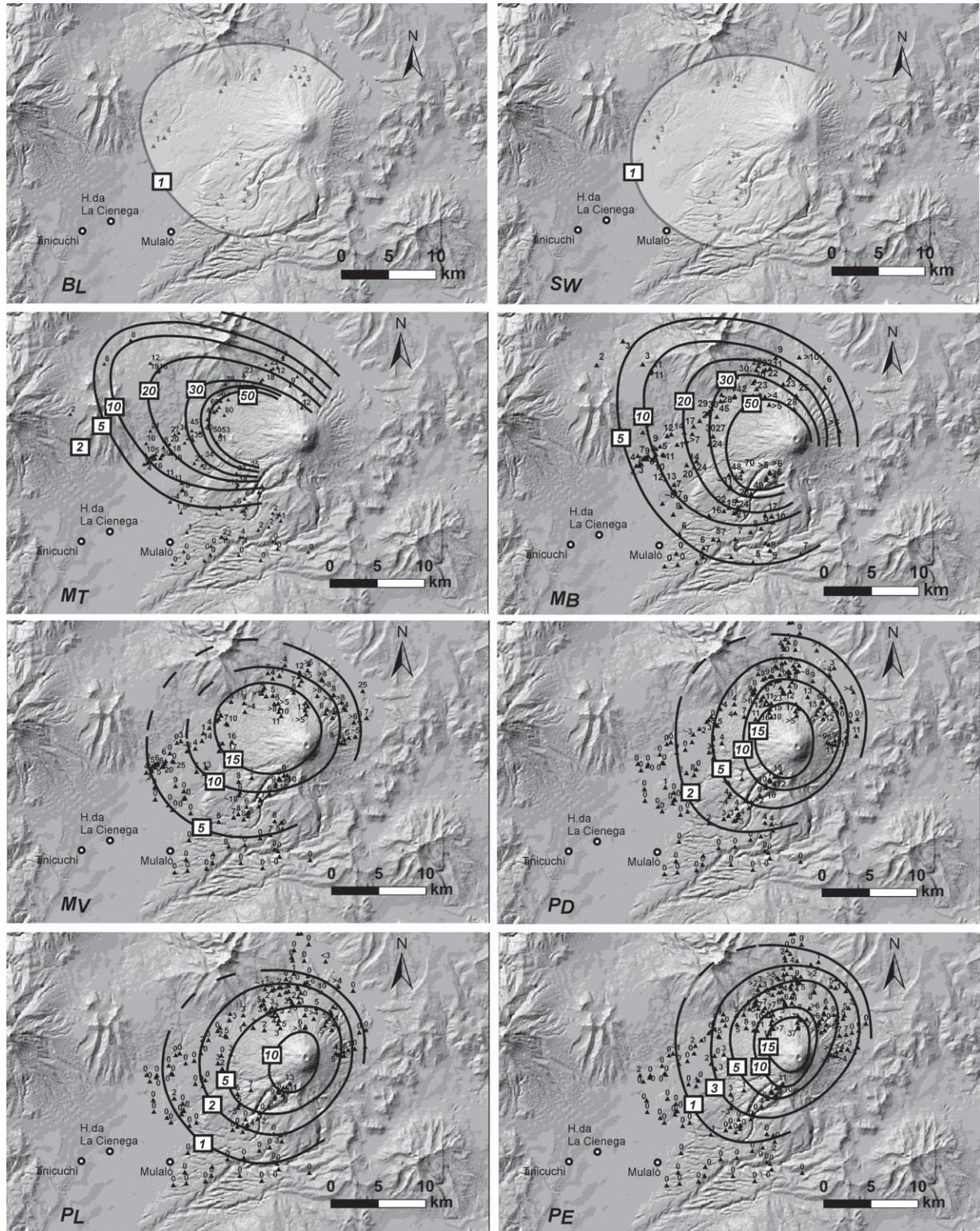


Figure 9. Isopach maps of fall beds of the Cotopaxi eruptions (with thickness in cm). Figures refer to layer M_T , layer M_B , layer M_V , layer P_D , layer P_L , and layer P_E . For layers B_L and S_W , only the general dispersal (1 cm isopach) of fallout deposits is presented. Labeled black triangles indicate thickness in each surveyed point.

three isopach lines because of the limited areal distribution of data. The volume estimate for this layer is therefore less accurate than for other layers. For the volume calculation, both exponential (Pyle, 1989; Fierstein and Nathenson, 1992) and power-law methods (Bonadonna and Houghton, 2005) were applied. The best-fit equations for the two methods are, respectively:

$$T = T_0 \exp(-k\sqrt{A}), \quad (1)$$

where the volume is calculated as

$$V = 13.08T_0 b_t^2, \quad (2)$$

and

$$T = T_{pl} A^{-m/2}, \quad (3)$$

where the volume is calculated as

$$V = \left[2T_{pl} \frac{\sqrt{A}^{(2-m)}}{2-m} \right]_0^\infty, \quad (4)$$

where T is the thickness, T_0 is the maximum thickness, b_t is the thickness half-distance, A is the area, k is the slope of the exponential fit, T_{pl} is the power-law coefficient, and m is the power-law exponent.

Integration of the power-law curve was done between $A_0^{1/2}$ (the distance of the maximum thickness of the deposit), and $A_{dist}^{1/2}$ (the distance of the extent of the deposit), because it is not possible to integrate the power-law curve between values of zero and infinity. Given that the variations of $A_0^{1/2}$ and $A_{dist}^{1/2}$ affect the final result, we used different values of $A_{dist}^{1/2}$ (100 or 200 km) and of $A_0^{1/2}$ (0.5 or 1) on the basis of the exponent of the fitting equations (>2 or <2) (Bonadonna and Houghton, 2005).

Exponential and power-law best fits for layers M_T , M_B , P_D , P_L , and P_E are compared in Figure 10. In most cases, distal trends are poorly constrained due to the lack of very distal outcrops. As a result, the two curve-fitting methods lead to different values (Table 6). Using the Pyle method, layers M_T and M_B have the largest volumes ($>0.12 \text{ km}^3$), while layer P_L , according with its limited dispersal, yielded a volume of 0.016 km^3 .

The power-law calculation provides volume estimates between 0.03 and 0.86 km^3 , i.e., 2–4 times larger than those calculated with Pyle's method. If distal data are missing or deposits have been eroded away, the power-law extrapolation should underestimate the volume less than the exponential fit (Bonadonna and Houghton, 2005). However, exponential trends appear to provide a better fit to the Cotopaxi data than

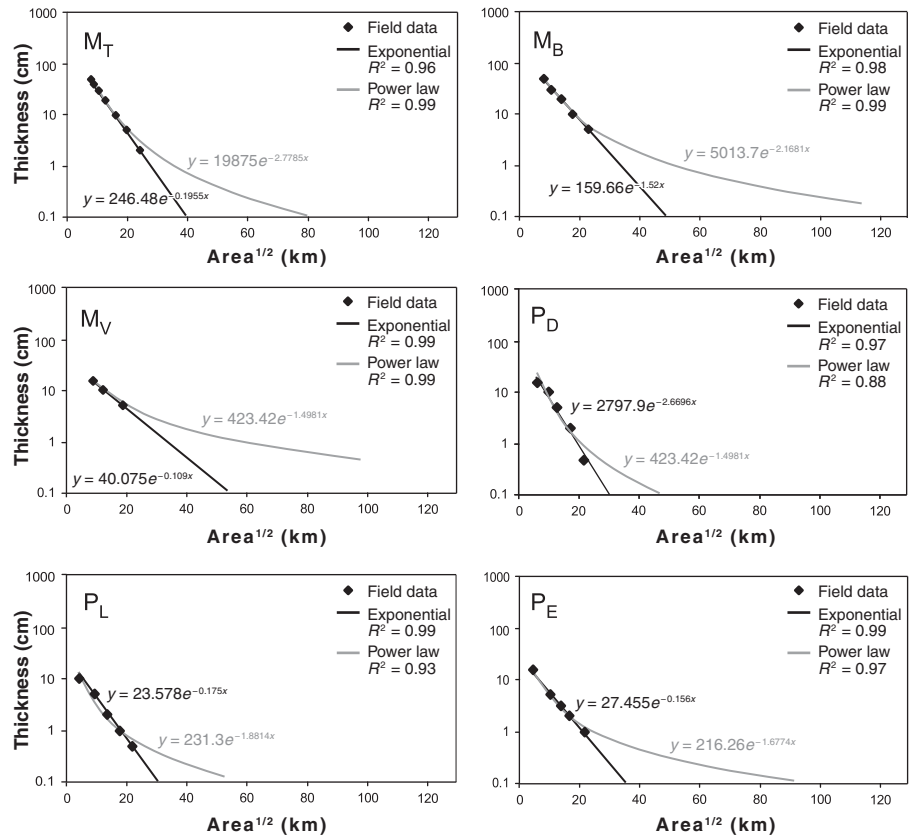


Figure 10. Plots of log thickness versus square root of area for six Cotopaxi fallout deposits, showing both exponential (black curves) and power-law (gray lines) best fits.

power-law trends; for this reason, we consider values from the power-law fit integration and from the exponential method as upper and lower limits, respectively.

According to Mothes (2006), layers M_T and M_B together comprise a volume of 0.40 km^3 (although no information regarding the calculation method is reported). We considered these two layers separately because they clearly represent different events with different dispersions

(Fig. 9). A summation of volume estimations for M_T and M_B to compare with Mothes' (2006) 0.40 km^3 estimate gives a higher mean value (1.03 km^3) from the power-law calculation, and a lower value from Pyle's method (0.27 km^3).

The extrapolated maximum thickness for layer P_E yields a value of 0.3 m , which is in good agreement with the values measured at the time of the eruption (Wolf, 1878). Small differences could depend on the fact that values reported

TABLE 6. VOLUME AND TOTAL MASS ESTIMATES OF COTOPAXI DEPOSITS

Layer	b_t value (km)	Exponential		Power law			
		Volume (m^3)	Total mass (kg)	Volume (m^3)	Total mass (kg)	$A_0^{1/2}$ (km)	$A_{dist}^{1/2}$ (km)
P_E	2.608	2.26×10^7	1.72×10^{10}	4.86×10^7	3.40×10^{10}	0.5	100
				6.34×10^7	4.44×10^{10}	0.5	200
P_L	2.30	1.54×10^7	1.14×10^{10}	3.14×10^7	2.20×10^{10}	0.5	100
				3.72×10^7	2.61×10^{10}	0.5	200
P_D	1.70	2.87×10^7	2.11×10^{10}	7.97×10^7	5.58×10^{10}	1	100
				1.29×10^8	9.03×10^{10}	0.5	100
M_V	3.58	6.74×10^7	4.71×10^{10}	1.58×10^8	1.11×10^{11}	0.5	100
				2.29×10^8	1.60×10^{11}	0.5	200
M_B	2.57	1.38×10^8	9.70×10^{10}	3.21×10^8	2.25×10^{11}	1	100
				3.95×10^8	2.77×10^{11}	0.5	100
M_T	2.00	1.29×10^8	9.05×10^{10}	4.96×10^8	3.48×10^{11}	1	100
				8.62×10^8	6.03×10^{11}	0.5	100

Note: Exponential method is from Pyle (1989), and the power-law method is from Bonadonna and Houghton (2005). Equations 1 to 4 are in the text; b_t values and proximal and outer integration limits ($A_0^{1/2}$ and $A_{dist}^{1/2}$) are also indicated.

by Wolf (1878) also considered ash thickness accumulated in the final stage of the 1877 event, which may not have been preserved.

Column Height Calculations

Little information on eruption column heights can be derived from historical documents that describe the eruptions (Table 1). Several techniques have been developed to determine this parameter from field measurements (e.g., distribution of maximum clast, deposit density, grain size). These measurements depend strongly on the method used in their collection, so that very different values of eruptive parameters are obtained depending on the field technique applied.

We determined the maximum clast size by averaging the three axes of the three largest clasts collected over a 0.5 m² sampling area; at each selected site, a 1-m-wide and 0.5-m-long hand-dug pit was surveyed for layers M_T, M_B, P_D, and P_E. Along natural vertical cuts, the sampling area was set, depending on the deposit thickness and horizontal length of the outcrop, to obtain a 0.5 m² horizontal area. Surveyed outcrops are distributed around the volcano between 2.8 km to 22 km from the vent (Fig. 11). Broken pumice clasts, which were abundant in layers M_T and M_B, were reconstructed by hand before measuring. In a few cases, large “outlier” clasts were observed and included in the data set.

Column heights were calculated with five different methods using maximum pumice and lithic clasts and isopleth area, crosswind range and downwind range (Carey and Sparks, 1986), median diameter and sorting of the deposits with the distance from the vent (Sparks et al., 1992), values of clast size and density of a clast as a function of maximum crosswind range (Wilson and Walker, 1987), and the theoretical predictions compared with observations of the column height and mass discharge rate used in Sparks (1986). Peak discharge rates of magma were calculated from column heights obtained from values of column heights calculated only with the Carey and Sparks (1986) method and by using the relationship in Sparks (1986).

Values of column height are summarized in Table 7. Layer M_B represents the highest intensity event of the post-twelfth-century activity of Cotopaxi, with a column height ranging from 25 to 36 km (considering the five different methods); layer M_T data show that this eruption was the second most intense (19 km to 32 km). Our field work showed that the scale of the eruptions that produced layers P_D and P_E was lower, both in terms of magnitude and intensity, than that of M_T and M_B: estimated column heights (19–23 km and 20–24 for layer P_D and P_E, respectively)

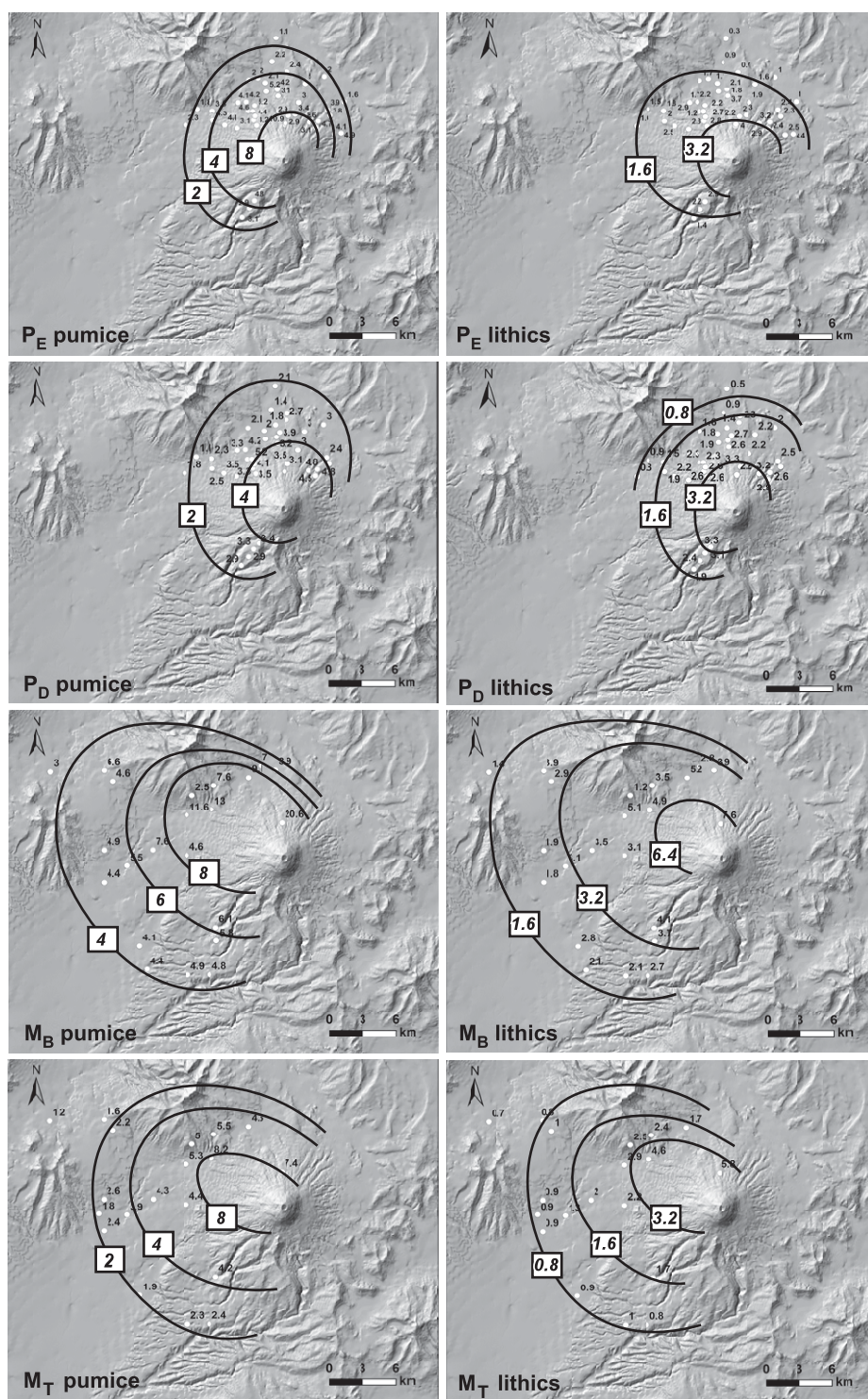


Figure 11. Isopleths (in cm) for layer P_E pumice and lithics, P_D pumice and lithics, M_B pumice and lithics, and M_T pumice and lithics. Numbers refer to measurements obtained by averaging the three axes of the three largest clasts accumulated over 0.5 m². Solid lines are the interpolation.

TABLE 7. COLUMN HEIGHTS OF MAIN FALLOUT LAYERS

Layer	Carey and Sparks (I) (1986)	Carey and Sparks (II) (1986)	Sparks et al. (1992)	Wilson and Walker (1987)	Sparks (1986)	H_T (min-max)	MDR (kg/s)
P_E	20	21	—	20	24	20–24	2.57×10^7
P_D	21	21	—	19	23	19–23	2.57×10^7
M_B	25	29	25	31	36	25–36	9.34×10^7
M_T	23	25	19	23	32	19–32	5.16×10^7
S_W	—	—	17	—	—	17	1.10×10^7
B_L	—	—	25	—	—	25	5.16×10^7

Note: All values are in km. Column height range (H_T) is also reported. Carey and Sparks I and II refer to maximum pumice and lithic clasts versus isopleths area and crosswind range versus downwind range, respectively. Maximum and minimum values obtained from different methods are reported on the right. MDRs (mass discharge rates, in kg/s) are calculated as $H = 0.295[M_0]^{0.25}$ (Sparks, 1986) from values of column heights calculated with Carey and Sparks II method.

confirm these observations. Column heights for layers B_L and S_W were calculated only with the method of Sparks et al. (1992); these values are considered to be minima. Since the Carey and Sparks method (crosswind range versus downwind range) is the most commonly used, hereafter, if possible, we will refer to this method for further discussion on column heights. For layers M_B and M_T , we obtained values similar to those obtained by Barberi et al. (1995) (29 km versus 30 km and 25 km versus 28 km, respectively).

Values of column height can be converted to magma discharge rates. The original equation of Wilson and Walker (1987) is strictly valid only for a plume temperature of 1120 K, appropriate for silicic magma. Wilson and Walker's (1987) equation can be modified for an eruption temperature of 1300 K, so that:

$$H = 0.295[M_0]^{0.25}, \quad (5)$$

where H is the maximum column height, and M_0 is the mass eruption rate (Sparks, 1986). Using this equation, we estimate mass eruption rates between 1.10×10^7 kg/s for layer S_W , which is consistent with its small dispersal, and 9.34×10^7 kg/s for layer M_B . Minimum durations of the eruptive events (Table 8) were obtained by dividing the calculated mass (Table 6) by the peak mass discharge rates. The lithic contribution was subtracted from the final mass value using lithic/juvenile ratios obtained from component analyses (Table 3). Estimated eruption durations are between 8.3 and 27.9 min if we use the mass obtained from the exponential method; by using

the mass obtained with the power-law method, estimates of eruption duration range from 19.0 to 146.6 min. Our estimates for the duration of the 1877 eruption range from 8.3 to 19 min; a very short paroxysmal phase for the 1877 eruption is consistent with descriptions in the historical chronicles.

Classification of the Events

Tephra deposition from eruption columns and the thinning rate of the associated deposits reflect variations in column height and wind speed. In terms of half-distance parameters (Pyle, 1989), eruptions with large b_c and low b_c/b_l (where b_c and b_l are the half-distance of the maximum clast size and maximum thickness, respectively) are the most widely dispersed. Using Pyle's (1989) classification scheme for tephra-fall deposits (Fig. 12), M_T and M_B lie in the field of Plinian eruptions (in agreement with their dispersal and column heights), while P_D and P_E plot in the field of sub-Plinian eruptions.

The erupted volume and eruption cloud heights can be used to determine the explosivity value (VEI) as described by Newhall and Self (1982). On the basis of column heights, both layers M_T and M_B rank as VEI 5 events (>25 km), whereas, if we consider ejecta volumes, they should be considered as a more realistic VEI 4 (as also suggested by Hall et al., 2004; Hall and Mothes, 2008; Mothes, 2006). Layer P_D and P_E rank as VEI 4 on the basis of column heights and VEI 3 for volumes of ejected products (>10,000,000 m³).

RECONSTRUCTION OF THE POST-TWELFTH-CENTURY ACTIVITY

The historical descriptions, when combined with a detailed study of extensively exposed tephra successions, have made it possible to create an accurate reconstruction of the past 800 yr of Cotopaxi eruptive history and assess the associated eruptive parameters. After the emplacement of the Quilotoa coignimbrite ash-fall blanket around A.D. 1140, Cotopaxi produced two midscale eruptions (tephra layers B_L and S_W) separated by a centuries-long period of quiescence during which a decimeter-thick soil bed formed. The three subsets of B_L tephra deposits suggest that the eruption started with a short-lived, violent explosion that disrupted a lava dome or plug. The explosion produced a north-directed pyroclastic density current that deposited a fines-poor to clast-supported tephra deposit (blast beds B_{LL} and B_{LU}). A sustained sub-Plinian phase (estimated column height of 25 km with a peak Mass Discharge Rate (MDR) of 5.16×10^7 kg/s) followed, depositing a pumice fallout bed in the southern sector of the volcano (upper subbed B_{LP}). No clear age indication can be derived for this event. The overlying tephra bed (S_W) had Plinian character, with an estimated column height of 17 km and a peak MDR of 1.10×10^7 kg/s. It possibly corresponds to the A.D. 1534 event narrated in the Spanish chronicles.

The 5.5-km-long Yanasacha lava tongue (0.05 km³) on the northern sector of the Cotopaxi cone is the only unequivocal lava flow emplaced during the investigated period. The flow was recognized by Barberi et al. (1995) to predate our M_T bed and postdate the S_W tephra. In agreement with Hall and Mothes (2008), we propose that the flow was emplaced following the final stage of B_L activity.

After a period marked by erosion and/or soil formation, activity resumed in the mid-eighteenth century with two Plinian eruptions associated with pyroclastic density currents. Both Plinian episodes were heralded by ash emission and dome extrusion, as suggested by ejection of thermally jointed (hot) lava clasts in the early phase of the eruptions. According to the chronicles, the 1742–1744 eruptions

TABLE 8. DURATION OF THE ERUPTIVE EVENTS CALCULATED USING THE MASS OF THE DEPOSITS (TABLE 6) AND THE MASS DISCHARGE RATES (TABLE 7)

Layer	MDR (kg/s)	Total mass exponent (kg)	Mass (juvenile) exponent (kg)	Duration (min)	Total mass power law (kg)	Mass (juvenile) power law (kg)	Duration (min)
P_E	2.57×10^7	1.72×10^{10}	1.30×10^{10}	8.3	3.92×10^{10}	2.95×10^{10}	19.0
P_D	2.57×10^7	2.11×10^{10}	1.68×10^{10}	10.8	7.31×10^{10}	5.50×10^{10}	35.5
M_B	9.34×10^7	9.70×10^{10}	9.30×10^{10}	16.5	2.51×10^{11}	1.89×10^{11}	42.7
M_T	5.16×10^7	9.05×10^{10}	8.67×10^{10}	27.9	4.76×10^{11}	3.58×10^{11}	146.6

Note: Total mass values (both from exponential and power-law method estimates) were converted to total juvenile mass according to the juvenile/lithic ratio (Table 3).

consisted of repeated, relatively short-lived Plinian episodes. Our recognition of multiple beds separated by surge deposits within the M_T tephra corresponds with the description of multiple bursts. This correlation is also supported by the recognition of lahar units within the fallout bed in a valley site along Rio Cutuchi. A maximum column height of 25 km is estimated for the entire M_T tephra set. This value must be regarded as a possible overestimation, because the cross-wind range of isopleths may represent the superposition of the deposits from different eruptive episodes. The cumulative isopachs yield a total volume of 0.13–0.86 km³. By considering a peak MDR of 5.16×10^7 kg/s, we obtain a maximum, cumulative duration of 147 min. The discovery of colonial roof tiles in lahar deposits associated with the event (Mothes et al., 2004) is consistent with the description of large-scale lahars generated by the 1742–1744 activity. Rapid snow-ice melting episodes were probably triggered by the flow of dilute density currents (surges) over the glacier; the resulting radially dispersed lahars were very rich in fine ash (inherited from the surges). The occurrence of glass-bearing, breadcrust bombs in these lahar deposits suggests that Vulcanian explosions may have been intercalated or associated with Plinian activity and pyroclastic surge by column collapse.

We link the overlying layer M_B to eruptions in 1766 and 1768 on the basis of historical accounts and ¹⁴C ages of the M_B -associated scoria flow (A.D. 1730–1810). The isopach and isopleth maps presented in this paper accord well with the description of bomb fallout in vil-

lages located close to the deposit dispersal axis. The M_B fallout bed was produced by the most intense Plinian column of the studied period (column height estimated at 29 km), with a volume of 0.13–0.39 km³. We estimate a total duration of 43 min (peak MDR of 9.34×10^7 kg/s), which matches with the description of the main event of April 1768. Scoria-flow deposits related to the M_B event (M_S deposits) were observed on the northern side of the cone both as widespread flows dispersed over fairly large areas (scoria flows produced by column collapse) and as small-volume, tongue-like, scoria-flow deposits concentrated within valleys, possibly related to late-stage boiling-over activity. At some localities, deposits show evidence of incipient welding and pronounced oxidation, suggesting emplacement at magmatic temperatures. We do not agree with the interpretation of Mothes and Hall (2008) that these deposits are lahar-related, because, in our opinion, oxidation of the top-most part of the deposits provides unequivocal evidence of air penetration into a still very hot, porous deposit.

Long-lasting (decades?), moderate-energy explosive activity started immediately after the 1768 eruption and generated substantial emissions of black ash that are collectively recorded by layer M_V (volume of 0.06–0.23 km³). The eruptive style that produced the M_V bed is unique in the studied period and possibly marks long-lasting activity that was dominated by extensive magma degassing. The distinctive, light-gray bed of fine glassy ash within the lower third of M_V (M_{VW}) is possibly the distal equivalent of the A.D. 1773 andesitic pumice and ash eruption

of Tungurahua volcano, located 87 km south (Robin et al., 1999).

After a few decades of quiescence, volcanic activity resumed in the mid-nineteenth century, producing a series of explosive events that emplaced three thin (a few centimeters thick), moderately distributed, fallout beds (P_D , P_L , and P_E). The layers are associated with (or followed by) narrow, valley-controlled, scoria-flow tongues produced by boiling-over activity. Layer P_D , in particular, consists of two pumice fallout beds (P_{DC} and P_{DF}) separated by a reddish ash layer (P_{DR}). We have related bed P_D to the 1853 activity on the basis of both the identification of scoria-flow deposits and the description of nueé ardentes in the chronicles. The scoria-flow deposits occur at the top of both layers P_{DC} and P_{DF} and they were recognized on both the northern and southern sides of the volcano. The P_D fall deposit has a volume of 0.03–0.13 km³ and estimated eruption duration of 35.5 min (peak MDR of 2.57×10^7 kg/s). Episodes of mild activity preceded the large 1877 eruption, as recorded by layer P_L , which is possibly attributed to an event in 1866. Alternatively, the layer may represent the starting phase of the 1877 activity. The 1877 eruption consisted of a Plinian column (centimeter-thick tephra bed P_E), followed by the emplacement of scoria-flow tongues (P_{ES} deposit). For this eruption, we estimated a column height of 21 km, equivalent to a peak mass discharge rate of 2.57×10^7 kg/s. Considering that the volume of the fallout deposit is 0.02–0.06 km³, the event must have lasted only a few tens of minutes. The field-based reconstruction of the duration and dispersal of the fallout event matches the description given in the chronicles. The short-lived climactic (sustained) phase started at 10 a.m. of 26 June and lasted only a few minutes. It was followed immediately by 15–30 min of boiling-over activity, consistent with the emplacement of scoria flow that poured to the north and northwest (e.g., Wolf, 1878).

After the 1877 event, activity decreased in both intensity and magnitude. Three thin ash layers (layer P_R) represent the last, post-1880 events reported in the chronicles.

Our reconstruction of the last five centuries activity only partly agrees with reconstructions of Barberi et al. (1995) and Hall and Mothes (2008). There is general agreement on the 1877 event and corresponding tephra layer. In contrast, deposits that we have attributed to eruptions in 1742–1744 (M_T) and 1766–1768 (M_B) were both attributed to the 1742–1744 events by Mothes et al. (2004) and Hall and Mothes (2008), whereas Barberi et al. (1995) attributed the M_T and M_B beds to the 1534 eruption.

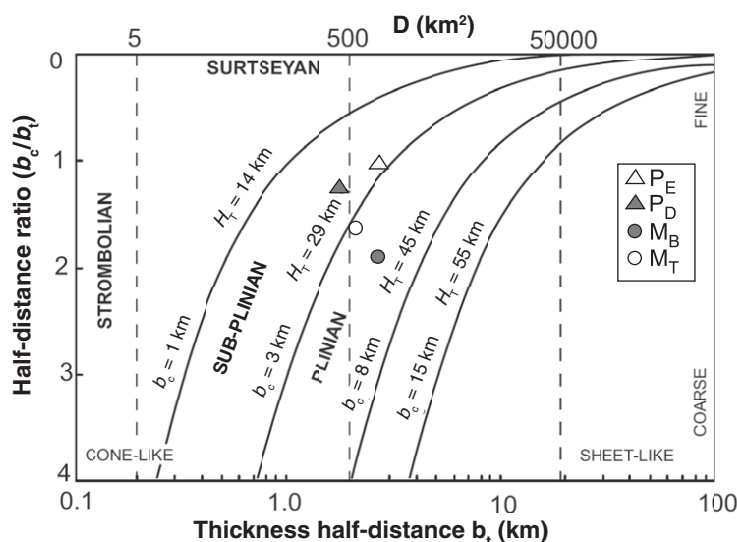


Figure 12. Classification scheme for tephra deposits introduced by Pyle (1989) showing the Plinian-sub-Plinian character of the four M_T , M_B , P_D , and P_E Cotopaxi deposits.

The recent period (nineteenth century) investigated by Hall and Mothes (2008) has a general tephra reconstruction and age attribution that fits with this work, although we could not, unequivocally, identify a lava flow on the western side of the volcano that they related to the 1853 eruption. In addition, ambiguity exists about the possible attribution of a tephra layer to an 1803 event that is reported by von Humboldt (Table 1).

DISCUSSION AND CONCLUSIONS

Based on extensive collection of field data around the volcano, coupled with historical information, new ^{14}C dates, and grain-size/componentry data of deposits, we propose a detailed and robust picture of the physical volcanology of Cotopaxi activity over the past 800 yr. The data presented in this work substantially upgrade the information made available by previous studies (Barberi et al., 1995; Mothes et al., 2004; Hall and Mothes, 2008), making the volcanic system of Cotopaxi one of the best known and documented worldwide in terms of eruptive history and physical volcanology parameters. In this way, we not only extend general knowledge of the behavior of andesitic volcanoes, but also provide new constraints on the specific eruptive history of Cotopaxi that will aid in hazard assessment.

Eruptive Behavior

Our data reveal two contrasting behaviors of Cotopaxi volcano over the past 800 yr: (1) During the period A.D. 1150–1742, the average magma eruption rate was low, and activity consisted of isolated explosive eruptions accompanied by the Yanasasha lava flow, and (2) during the period A.D. 1742–1880, the average magma eruption rate was much higher ($\sim 10^9$ – 10^{10} kg/yr), and activity was dominated by numerous explosive events separated by eruptive pauses that lasted from a few years to a few decades (eruption cluster). The eighteenth- to nineteenth-century cluster started with Plinian outbursts fed by fairly evolved magma (A.D. 1742–1744), followed by very high intensity and magnitude Plinian bursts that were fed by less evolved magma (A.D. 1766–1768). These large Plinian events were eventually followed by a period of long-lasting, moderate-intensity magma degassing mixed with staggered, low-intensity and low-magnitude explosive bursts, each dominated by a short-lived sub-Plinian phase followed by boiling-over activity and associated scoria flows.

Barberi et al. (1995) assumed that the eruptive behavior of Cotopaxi over the past 2000 yr was

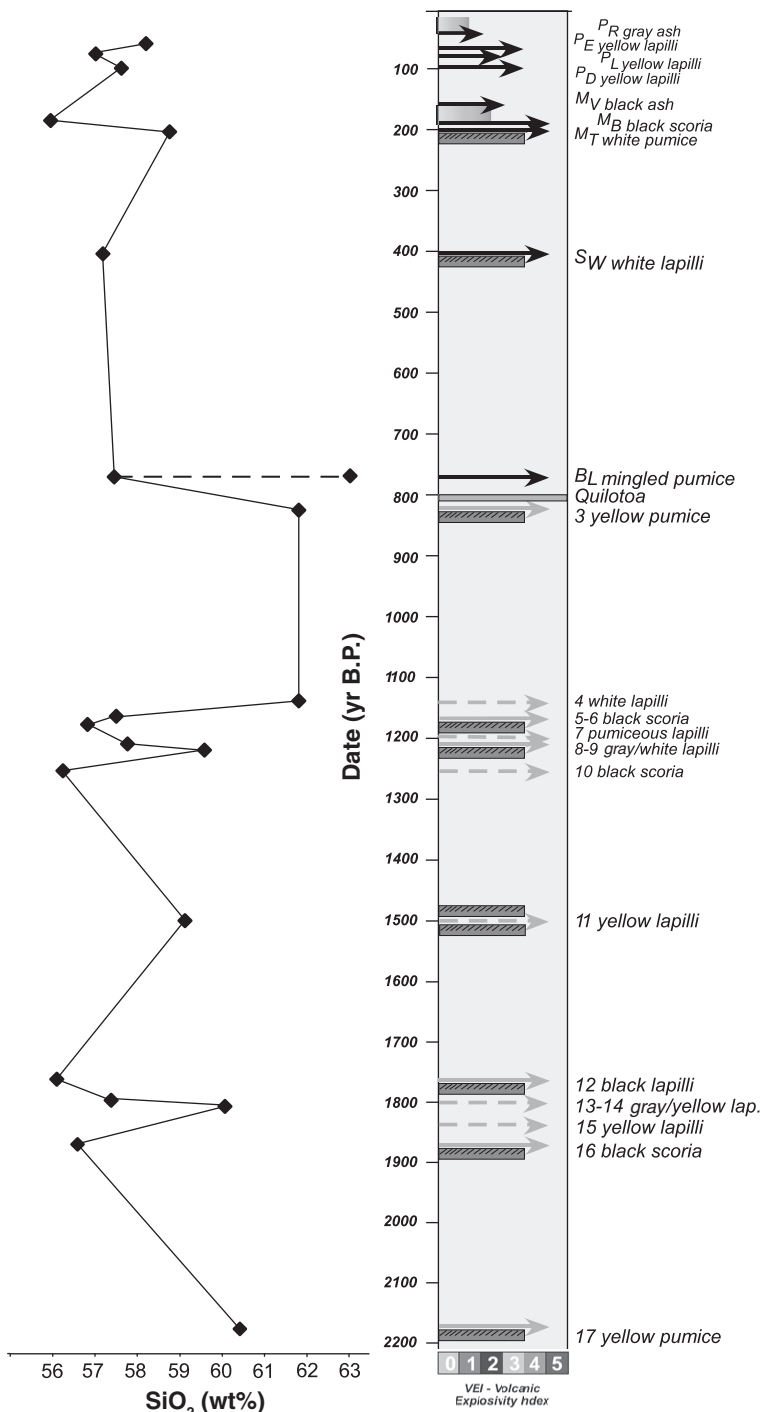


Figure 13. Schematic chronogram of Cotopaxi activity during the past 2000 yr. Black arrows refer to explosive eruptions studied in this work; length reflects the estimated volcanic explosivity index (VEI). Shaded boxes show periods of persistent ash emission. Gray arrows are data from Barberi et al. (1995), all arbitrarily considered as VEI 4. Gray dashed arrows are undated explosive eruptions repositioned in this work (originally arbitrarily placed at regular intervals between two dated events); gray solid lines correspond to dated events. Soil beds are indicated as dark-gray striped boxes. SiO_2 variations are also reported on the left. For layer B_L , both compositions of mingled portions are reported.

characterized by evenly spaced activity, with an average of one eruption every 117 yr. The average recurrence time was obtained by simply dividing the time lapse of 2000 yr by the number of tephra beds counted in the same interval. We have revised this first-order approximation in the light of our results for the past 800 yr of activity, which show that the volcano's activity has been characterized both by periods of very frequent, low- to high-intensity activity, and by scattered, mid- to high-intensity eruptions separated by long repose periods.

The new data led us to reconsider the significance of ^{14}C ages presented in Barberi et al. (1995), particularly by examining evidence for the presence and thickness of humic-rich soil beds, and/or important erosional surfaces separating the single layers. We have done this using the original field observations and notes of one of us (Mauro Rosi), a coauthor on the Barberi et al. (1995) paper. We have used the most complete stratigraphic logs, that is, those comprising all of the 2000–800 yr B.P. deposits (from unit 17–3; Barberi et al., 1995). If we assume that soil thickness is a first-order proxy for the duration of eruptive quiescence, it is possible to reconstruct a complete stratigraphy of the deposits in which eruption clusters (with no obvious intervening soils) are separated by long periods during which only a few large eruptions occur (Fig. 13).

This pattern of eruption recurrence is similar to the patterns that we observe during the past 800 yr of activity. In our opinion, clustering of eruption activity at Cotopaxi is critical to bear in mind for the construction of a model behavior for the volcano. As suggested by ^{14}C data, these clusters have a maximum duration no longer than 100–120 yr. In particular, events 16–12 and 10–5 of Barberi et al. (1995) represent clusters that are characterized by the initial eruption of mafic scoriae of andesitic composition.

Our study also provides evidence of some peculiar features in the activity of the volcano during the last centuries that contrast with the activity of the preceding two millennia. In particular, the last eruption cluster was initiated by two large-intensity/magnitude events (M_T and M_B), followed by several small events that are either poorly preserved or not recognized in distal outcrops. For this reason, our critical review of the stratigraphic logs of Barberi et al. (1995) included examination of the record for the possible occurrence of small-scale events scattered between the larger eruptions. Even in the numerous proximal sections, however, the deposits of past activity seem to not record the occurrence of sub-Plinian to Vulcanian events. The completeness of the examined outcrops, as well as the large number of natural exposures in

the plains at the foot of the cone, makes us confident that a change in the style of activity has occurred during the last three centuries.

A Possible Model of Behavior

It is recognized that activity of frequently erupting, central volcanoes ranges from fairly uniform (relatively rare) to unevenly spaced (common). It is also considered likely that the eruptive frequency is a function of the way magma is supplied from depth and stored in shallow plumbing/magma chamber systems. Data on time scales of magma transport and storage are rather scarce, as they require knowledge of several parameters (age, volume, and eruptive parameters). Despite this limitation, nonuniform time spacing of eruptions is well known and has been described, for example, over millennia at Vesuvius (Cioni et al., 2008; Santacroce et al. 2008) and on time scales of single eruptive episodes at Mount St. Helens (e.g., Scandone et al., 2007) or at Montserrat (Elsworth et al., 2008).

Although we cannot rule out that tectonic activity can influence the intrusion and extrusion rates, and that the stress field in the upper middle crust can facilitate the ascent of mafic magmas and influence the extrusion rate (Martin and Rose, 1981; Bacon, 1982), we suggest that variations in eruption frequency, intensity, magnitude, and composition recorded in the Cotopaxi stratigraphy probably reflect modulation in the magma supply rate from depth. We illustrate this using a diagram of cumulative eruptive vol-

ume through time (Fig. 14). Although the volume of pyroclastic flows and domes is not taken into account, the diagram highlights the observation that during periods of high magma supply, eruption clusters correspond to periods of high eruptive rate. Because the first eruptions of these clusters are often associated with the emission of large volumes of poorly evolved, andesitic magma, we suggest that these periods are triggered by an increase of magma supply from depth. The high intensity generally associated with these eruptions may reflect the primitive, volatile-rich nature of magma feeding the shallow plumbing system of the volcano. Longer periods of inactivity that end with large eruptions of mildly to highly evolved magmas could result from periods of lower magma supply, during which magma accumulates and evolves in a shallow reservoir before reaching the conditions needed to trigger an eruption (volatile supersaturation, overpressurization due to rapid melt volume increase in the reservoir, etc.).

Clusters of eruptive activity are common at basaltic central volcanoes, where such behavior is explained by deep intermittent magma supply (periods of sustained feeding of upper-crustal magma storage regions) that alternate with periods of low or no supply (Shaw and Chouet, 1991). In this category we can include Kilauea volcano, Hawaii (including the current phase of activity of pu'u o'o) (Dvorak and Dzurisin, 1993), Mount Etna, Italy, which from 1971 on has shown an average supply rate much higher than the pre-1971 period (Wadge et al., 1975; Andronico and Lodato, 2005), and

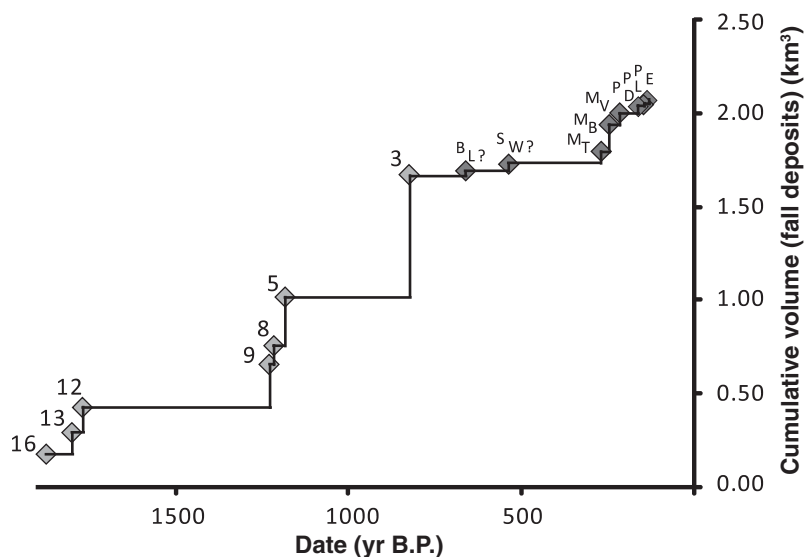


Figure 14. Cumulative volume (km^3) of tephra fall deposits versus time for the past 2000 yr of activity at Cotopaxi. Dark-gray diamonds are data from this work; light-gray diamonds are from Barberi et al. (1995). Label of each layer is also indicated.

Krafla volcano, Iceland, which experienced a period of intensive feeding that has been followed by a phase of substantial quiescence (Takada, 1999).

Similar behaviors are possible at andesitic central volcanoes. Deep refilling processes are crucial for the evolution of magma chambers, in particular, in recharging shallow systems through injection of magma and volatiles directly from the source region or from “lower stage,” deeper crustal reservoirs (e.g., Tungurahua and Soufrière Hills volcanoes, both of which currently seem to be experiencing an input of deep mafic magma; e.g., Bons and van Milligen, 2001; Hall et al., 2008; Humphreys et al., 2010).

The critical revision of the past 2000 yr of explosive activity of Cotopaxi that we have summarized here provides a starting point for discussing the range of eruption scenarios that might constitute the next eruptive event. A simple statistical approach to volcano behavior (e.g., Barberi et al., 1995) can only be considered a first-order approximation; a more detailed assessment of the eruptive behavior would require including observed temporal variations in the eruptive frequency and magnitude/intensity of eruptive events that the volcano has shown over the last two millennia. From this perspective, we suggest that renewed magmatic unrest could foreshadow either a single low- to medium intensity explosive eruption or initiation of a new cluster of eruptions that are closely spaced in time. We emphasize that all the relevant information highlighted by this work may apply not only to Cotopaxi but to other volcanoes worldwide and should be considered when trying to use information on past activity as a tool to evaluate the probability of occurrence of a given eruption type in the future. Also, we suspect that eruptions may be clustered more often than they are equally spaced, and this work thus helps in providing a new interpretation for the ways in which stratovolcanoes work.

ACKNOWLEDGMENTS

Funding for the research was provided by a PRIN-MIUR (Progetti di Ricerca di Interesse Nazionale—Ministero dell’Istruzione, dell’Università e della Ricerca) 2005 grant (scientific principal investigator M. Rosi) and a grant to R. Cioni provided by Regione Sardegna (Italy). K.V. Cashman was funded by a National Science Foundation (NSF) grant (EAR-0510437). The authors would also like to thank the ESPE (Escuela Politécnica del Ejército) for logistical and technical help during the field work, and C. Bonadonna and the Geneva team for thoughtful discussions on eruptive dynamics. Laboratory facilities were kindly made available by M. Lezzerini and F. Colarieti. The manuscript was improved by helpful reviews from A. di Muro, M. Ort, and L. Ferrari.

REFERENCES CITED

- Almeida, E., 1995, Flujos de lodo del volcán Cotopaxi: Quito, Instituto Geográfico Militar, Revista Geográfica, v. 34, p. 153–162.
- Andronico, D., and Lodato, L., 2005, Effusive activity at Mount Etna volcano (Italy) during the 20th century: A contribution to volcanic hazard assessment: *Natural Hazards*, v. 36, p. 407–443, doi: 10.1007/s11069-005-1938-2.
- Annen, C., Blundy, J.D., and Sparks, R.S.J., 2006, The genesis of intermediate and silicic magmas in deep crustal hot zones: *Journal of Petrology*, v. 47, p. 505–539, doi: 10.1093/petrology/egi084.
- Archivo Nacional, 1768, Serie Haciendas, 1768; Temporalidades 1768: Quito, Ecuador, Libro de Cuentas Hacienda El Pedregal; Inventario y Producción-Chillo 1768, 208 p.
- Arzobispal, A., 1885, Boletín del Instituto de Historia Eclesiástica Ecuatoriana: Quito, Ecuador, v. 18 (1998), p. 13–37.
- Athens, J.S., 1999, Volcanism and archaeology in the northern highlands of Ecuador, in Mothes, P., ed., *Actividad volcánica y pueblos precolombinos en el Ecuador*: Quito, Ecuador, Abya-Yala, p. 157–190.
- Avendaño, J., 1985, Imagen del Ecuador, Economía y Sociedad Vistas por un Viajero del Siglo XIX: Quito, Corporación Editora Nacional, 1985, p. 102–106.
- Bacon, C.R., 1982, Time-predictable bimodal volcanism in the Coso Range, California: *Geology*, v. 10, p. 65–69, doi: 10.1130/0091-7613(1982)10<65:TBVITC>2.0.CO;2.
- Bacon, C.R., and Lanphere, M.A., 2006, Eruptive history and geochronology of Mount Mazama and the Crater Lake region, Oregon: *Geological Society of America Bulletin*, v. 118, p. 1331–1359, doi: 10.1130/B25906.1.
- Barberi, F., Coltelli, M., Frullani, A., Rosi, M., and Almeida, E., 1995, Chronology and dispersal characteristics of recently (last 5000 years) erupted tephra of Cotopaxi (Ecuador): Implications for long-term eruptive forecasting: *Journal of Volcanology and Geothermal Research*, v. 69, p. 217–239, doi: 10.1016/0377-0273(95)00017-8.
- Barriga, F., 1973, Monografía de la Provincia de Cotopaxi. Volume 2: Ambato, Ecuador, Editorial Primicias, 97 p.
- Bonadonna, C., and Houghton, B.F., 2005, Total grain-size distribution and volume of tephra-fall deposits: *Bulletin of Volcanology*, v. 67, p. 441–456, doi: 10.1007/s00445-004-0386-2.
- Bons, P.D., and van Milligen, B.P., 2001, New experiment to model self-organized critical transport and accumulation of melt and hydrocarbons from their source rocks: *Geology*, v. 29, no. 10, p. 919–922, doi: 10.1130/0091-7613(2001)029<0919:NETMSO>2.0.CO;2.
- Bourdon, E., Eissen, J.-P., Gutscher, M.-A., Monzier, M., Hall, M.L., and Cotton, J., 2003, Magmatic response to early aseismic ridge subduction: The Ecuadorian margin case (South America): *Earth and Planetary Science Letters*, v. 205, p. 123–138, doi: 10.1016/S0012-821X(02)01024-5.
- Carey, S., and Sparks, R.S.J., 1986, Quantitative models of the fallout and dispersal of tephra from volcanic eruption columns: *Bulletin of Volcanology*, v. 48, p. 109–125, doi: 10.1007/BF01046546.
- Cedulario de Latacunga: anonymous author, unknown date. Document reviewed and cited by von Humboldt (1837); Wolf (1878); and Zúñiga (1989).
- Cicala, M.S.I., 1994, Descripción histórico-topográfica de la Provincia de Quito de la Compañía de Jesús: Quito, Biblioteca Ecuatoriana “Aurelio Espinosa Pólit,” 1994, p. 134, 227, 337–338.
- Cieza de León, P., 1553, The Second Part of the Chronicle of Peru, translated by Clements R. Markham: London, Hakluyt Society, 1883 (reissued by Cambridge University Press, 2010; ISBN 9781108011617).
- Cioni, R., Bertagnini, A., Santacroce, R., and Andronico, D., 2008, Explosive activity and eruption scenarios at Somma-Vesuvius (Italy): Towards a new classification scheme: *Journal of Volcanology and Geothermal Research*, v. 178, p. 331–346, doi: 10.1016/j.jvolgeores.2008.04.024.
- Coba, J., 1929, Monografía General del Cantón Píllaro: Quito, Prensas Católica, p. 232–235.
- Crandell, D.R., 1987, Deposits of Pre-1980 Pyroclastic Flows and Lahars from Mount St. Helens Volcano, Washington: U.S. Geological Survey Professional Paper 1444, 91 p.
- de Herrera, A., 1601–1615, Historia General de los Hechos de los Castellanos en las Islas y Tierra Firme del Mar Océano: Madrid, 4 volumes.
- de Zárate, A., 1555, Historia del Descubrimiento y Conquista de las Provincias del Perú, in *Bibl. Aut. Esp.*, Vol. XXVI, Madrid, 1947, 312 p.
- Diguja, J., 1768, Carta del Presidente de Quito al Rey de España, del 20 de abril, in *Wolf* (1878), Appendix 13; Guayaquil, Ecuador, Imprenta de El Comercio, p. 116–120.
- Di Muro, A., Rosi, M., Aguilera, A., Barbieri, R., Massa, G., Mundula, F., and Pieri, F., 2008a, Transport and sedimentation dynamics of transitional explosive eruption columns: The example of the 800 BP Quilotoa Plinian eruption (Ecuador): *Journal of Volcanology and Geothermal Research*, v. 174, p. 307–324, doi: 10.1016/j.jvolgeores.2008.03.002.
- Di Muro, A., Pallister, J., Villemant, B., Newhall, C., Semet, M., Martínez, M., and Mariet, C., 2008b, Pre-1991 sulfur transfer between mafic injections and dacite magma in the Mt. Pinatubo reservoir: *Journal of Volcanology and Geothermal Research*, v. 175, p. 517–540.
- Dvorak, J.J., and Dzurisin, D., 1993, Variations in magma supply rate at Kilauea volcano, Hawaii: *Journal of Geophysical Research*, v. 98, p. 22,255–22,268.
- Eichelberger, J.C., Izbekov, P.E., and Browne, B.L., 2006, Bulk chemical trends at arc volcanoes are not liquid lines of descent: *Lithos*, v. 87, p. 135–154.
- El Becerro de Hijuelas or “El Becerro de Oro” de Latacunga, 1850, Manuscript by José Gómez de Araujo; two volumes: Latacunga, Biblioteca del Colegio Vicente León, 309 p.
- Elsworth, D., Mattioli, G., Taron, J., Voight, B., and Herd, R., 2008, Implications of magma transfer between multiple reservoirs on eruption cycling: *Science*, v. 322, p. 246–248, doi: 10.1126/science.1161297.
- Fernández de Oviedo y Valdes, G., 1526, Historia General y Natural de las Indias: Madrid, Biblioteca de Autores Españoles, 5 volumes, 654 p.
- Fierstein, J., and Nathenson, M., 1992, Another look at the calculation of fallout tephra volumes: *Bulletin of Volcanology*, v. 54, p. 156–167, doi: 10.1007/BF00728005.
- Fisher, R.V., 1961, Proposed classification of volcanoclastic sediments and rocks: *Geological Society of America Bulletin*, v. 72, p. 1409–1414, doi: 10.1130/0016-7606(1961)72[1409:PCOVSA]2.0.CO;2.
- Fisher, R.V., and Schmincke, H.-U., 1984, *Pyroclastic Rocks*: Berlin, Springer-Verlag, 472 p.
- Folk, R.L., and Ward, W.C., 1957, Brazos River bar: A study in the significance of grain size parameters: *Journal of Sedimentary Petrology*, v. 27, p. 3–26.
- González Suárez, F., 1970, Historia del Ecuador: Quito, Reedicción Casa de la Cultura Ecuatoriana, 374 p.
- Hall, M., 1977, El Volcanismo en el Ecuador: Quito, Instituto Panamericano de Geografía e Historia, 120 p.
- Hall, M., 1987, Peligros potenciales de las erupciones futuras del volcán Cotopaxi: Escuela Politécnica Nacional Monografía de Geología 5/12, p. 41–80.
- Hall, M., and Mothes, P., 2008, The rhyolitic–andesitic eruptive history of Cotopaxi volcano, Ecuador: *Bulletin of Volcanology*, v. 70, p. 675–702, doi: 10.1007/s00445-007-0161-2.
- Hall, M., and von Hillebrandt, C., 1988, Mapa de los Peligros Volcánicos Potenciales Asociados con el Volcán Cotopaxi: Zona Norte: Quito, Ecuador, Instituto Geofísico, Escuela Politécnica Nacional, scale 1:50 000.
- Hall, M., Mothes, P., and Samaniego, P., 2004a, The rhyolitic–andesitic history of Cotopaxi volcano, Ecuador, in *Proceedings of the IAVCEI (International Association of Volcanology and Chemistry of the Earth’s Interior) General Assembly 2004—Nov. 14–19: Pucón, Chile*.
- Hall, M., Mothes, P., Samaniego, P., and Yepes, H., 2004b, Eruption scenarios for Cotopaxi volcano, Ecuador, deduced from tephrochronology and historical accounts, in *Proceedings of the IAVCEI (International Association of Volcanology and Chemistry of*

- the Earth's Interior) General Assembly 2004—Nov. 14–19, Pucón, Chile.
- Hall, M., Mothes, P., Samaniego, P., Yepes, H., and Andrade, D., 2004c, Mapa Regional de Peligros Volcánicos Potenciales del Volcán Cotopaxi—Zona Norte y Zona Sur: Quito, IG-EPN (Instituto Geofísico—Escuela Politécnica Nacional) and Instituto Geográfico Militar, scale 1:50 000.
- Hall, M.L., Samaniego, P., Le Pennec, J.L., and Johnson, J.B., 2008, Ecuadorian Andes volcanism: A review of late Pliocene to present activity: *Journal of Volcanology and Geothermal Research*, v. 176, p. 1–6, doi: 10.1016/j.jvolgeores.2008.06.012.
- Hantke, G., 1951, Uebersicht ueber die vulkanische taetigkeit 1941 1947: *Bulletin Volcanologique*, v. II/IX 1951, 173 p.
- Hantke, G., and Parodi, I., 1966, Colombia, Ecuador and Peru: Catalogue of active volcanoes of the world and Solfataras Fields, Rome: IAVCEI (International Association of Volcanology and Chemistry of the Earth's Interior), v. 19, p. 1–73.
- Hildreth, W., and Lanphere, M.A., 1994, Potassium-argon geochronology of a basalt-andesite-dacite arc system: The Mount Adams volcanic field, Cascade Range of southern Washington: *Geological Society of America Bulletin*, v. 106, p. 1413–1429, doi: 10.1130/0016-7606(1994)106<1413:PAGOAB>2.3.CO;2.
- Hradecka, L., Hradecky, P., Kruta, M., Lysenko, V., Milcoch, B., and Paulo, A., 1974, La Exploración Geológica de Volcán Cotopaxi en el Ecuador: Prague, Czech Republic, Instituto Geológico Central, 61 p.
- Humphreys, M.C.S., Edmonds, M., Christopher, T., and Hards, V., 2010, Magma hybridisation and diffusive exchange recorded in heterogeneous glasses from Soufriere Hills volcano, Montserrat: *Geophysical Research Letters*, v. 37, doi: 10.1029/2009GL041926.
- Inman, D.L., 1952, Measures for describing the size distribution of sediments: *Journal of Sedimentary Petrology*, v. 22, p. 125–145.
- Kolberg, J., 1996, Hacia el Ecuador, Relatos de Viaje: Quito, Ediciones Abya-Yala, Colección Tierra Incógnita 17, 501 p.
- Kratzmann, D.J., Carey, S., Scasso, R., and Naranjo, J.A., 2009, Compositional variations and magma mixing in the 1991 eruptions of Hudson volcano, Chile: *Bulletin of Volcanology*, v. 71, p. 419–439, doi: 10.1007/s00445-008-0234-x.
- La Condamine, Ch.M., 1751, Diario del Viaje al Ecuador. Introducción Histórica a la Medición de los Tres Primeros Grados del Meridiano: Coloquio "Ecuador 1986": Quito, Ecuador, Editorial Publitécnica, translated by Eloy Soria Sánchez (1986), 222 p.
- Le Bas, M.J., Le Maitre, R.W., Streckeisen, A., and Zanettin, B., 1986, A chemical classification of volcanic rocks based on the total alkali-silica diagram: *Journal of Petrology*, v. 27, p. 745–750.
- López de Gómara, F., 1552, Historia General de las Indias y Conquista de México: editorial Porrúa ISBN 970-07-7021-4, Saragossa, 172 p.
- Martin, D.P., and Rose, W.I., 1981, Behavior patterns of Fuego volcano, Guatemala: *Journal of Volcanology and Geothermal Research*, v. 10, p. 67–81, doi: 10.1016/0377-0273(81)90055-X.
- Martínez, A., 1994, Pioneros y Precursores del Andinismo Ecuatoriano. Tomo I: Quito, Reedicción, Editorial Abya-Yala, p. 104, 193.
- Miller, C., Mullineaux, D., and Hall, M., 1978, Reconnaissance Map of Potential Volcanic Hazard from Cotopaxi Volcano, Ecuador: U.S. Geological Survey Miscellaneous Investigation Map I-1702, scale 1:50 000.
- Mothes, P., 1992, Lahars of Cotopaxi volcano, Ecuador: Hazard and risk evaluation, in McCall, G., Laming, D., and Scott, S., eds., *Geohazards, Natural and Man-Made*: London, Chapman and Hall, p. 53–64.
- Mothes, P., 2006, Cotopaxi Volcano and the Surrounding Valleys: Cities on Volcanoes 4: Intra-Meeting Field Trip Guide (23–27 January 2006): Quito, Ecuador, IAVCEI (International Association of Volcanology and Chemistry of the Earth's Interior), 30 p.
- Mothes, P.A., and Hall, M.L., 1999, Quilotoa's 800 y BP ash: A valuable stratigraphic marker unit for the integration period, in Mothes, P., ed., *Actividad Volcánica y Pueblos Precolombinos en el Ecuador*: Quito, Ecuador, Ediciones Abya-Yala, p. 111–138.
- Mothes, P.A., and Hall M.L., 2008, The Plinian fallout associated with Quilotoa's 800 yr BP eruption, Ecuadorian Andes: *Journal of Volcanology and Geothermal Research*, v. 176, p. 56–69.
- Mothes, P.A., Hall, M.L., and Janda, R.J., 1998, The enormous Chillós Valley lahar: An ash-flow-generated debris flow from Cotopaxi volcano, Ecuador: *Bulletin of Volcanology*, v. 59, p. 233–244, doi: 10.1007/s004450050188.
- Mothes, P., Hall, M.L., Andrade, D., Samaniego, P., Pierson, T.C., Gorki Ruiz, A., and Yepes, H., 2004, Character, stratigraphy and magnitude of historical lahars of Cotopaxi volcano (Ecuador): *Acta Vulcanologica*, v. 16, no. 1–2, p. 85–108.
- Mullineaux, D.R., 1996, Pre-1980 Tephra-Fall Deposits Erupted from Mount St. Helens, Washington: U.S. Geological Survey Professional Paper 1563, 99 p.
- Mullineaux, D.R., and Crandell, D.R., 1981, The eruptive history of Mount St. Helens., in Lipman, P.W., and Mullineaux, D.R., eds., *The 1980 Eruptions of Mount St. Helens*, Washington: U.S. Geological Survey Professional Paper 1250, 844 p.
- Nakamura, K., 1964, Volcano-stratigraphic study of Oshima Volcano, Izu: *Bulletin of Earthquake Research Institute*, v. 42, p. 649–728.
- Neri, A., Aspinall, W.P., Cioni, R., Bertagnini, A., Baxter, P.J., Zuccaro, G., Andronico, D., Barsotti, S., Cole, P.D., Esposito Ongaro, T., Hincks, T.K., Macedonio, G., Papale, P., Rosi, M., Santacroce, R., and Woo, G., 2008, Developing an event tree for probabilistic hazard and risk assessment at Vesuvius: *Journal of Volcanology and Geothermal Resources*, v. 178, p. 397–415.
- Newhall, C.G., and Self, S., 1982, The volcanic explosivity index (VEI): An estimate of explosive magnitude for historical volcanism: *Journal of Geophysical Research*, v. 87, p. 1231–1238.
- Parédez, E., 1982, Cotopaxi, Documentos de Oro: Quito, Editorial Cotopaxi, 191 p.
- Pyle, D.M., 1989, The thickness, volume and grain size of tephra fall deposits: *Bulletin of Volcanology*, v. 51, p. 1–15, doi: 10.1007/BF01086757.
- Reiss, W., 1874, Ueber Lavastrome der Tungurahua und Cotopaxi: *Zeitschrift der Deutschen Geologischen Gesellschaft*, v. 26, p. 907–927.
- Reiss, W., and Stübel, A., 1869–1902, *Das Hochgebirge der Republik Ecuador II*: Berlin, Petrographische Untersuchungen des Ostkordillere, 236 p.
- Robin, C., Hall, M.L., Beate, B., Mothes, P., and Monzier, M., 1999, Tungurahua Volcano, Ecuador: Structure, eruptive history and hazards: *Journal of Volcanology and Geothermal Research*, v. 91, p. 1–21, doi: 10.1016/S0377-0273(99)00047-5.
- Santacroce, R., Cioni, R., Marianelli, P., Sbrana, A., Sulpizio, R., Zanchetta, G., Donahue, D., and Joron, J.L., 2008, Age and whole rock-glass compositions of proximal pyroclastics from the major explosive eruptions of Somma-Vesuvius: A review as a tool for distal tephrostratigraphy: *Journal of Volcanology and Geothermal Research*, v. 177, no. 1, p. 1–18, doi: 10.1016/j.jvolgeores.2008.06.009.
- Sauer, W., 1965, *Geología del Ecuador*: Quito, Ecuador, Ministerio Educación, 383 p.
- Scandone, R., Cashman, K.V., and Malone, S.D., 2007, Magma supply, magma ascent and the style of volcanic eruptions: *Earth and Planetary Science Letters*, v. 253, p. 513–529, doi: 10.1016/j.epsl.2006.11.016.
- Schmid, R., 1981, Descriptive nomenclature and classification of pyroclastic deposits and fragments: Recommendations of the IUGS Subcommittee of the Systematics of Igneous Rocks: *Geology*, v. 9, p. 41–43, doi: 10.1130/0091-7613(1981)9<41:DNACOP>2.0.CO;2.
- Shaw, H.R., and Chouet, B., 1991, Fractal hierarchies of magma transport in Hawaii and critical self-organization of tremor: *Journal of Geophysical Research*, v. 96, no. B6, p. 10,191–10,207, doi: 10.1029/91JB00771.
- Sigurdsson, H., and Sparks, S.R.J., 1978, Rifting episode in North Iceland in 1874–1875 and the eruptions of Askja and Sveinagja: *Bulletin of Volcanology*, v. 41, no. 3, p. 149–167.
- Simkin, T., Siebert, L., McClelland, L., Bridge, D., Newhall, C., and Latter, J.H., 1981, *Volcanoes of the World*: Stroudsburg, Pennsylvania, Hutchinson Ross, 233 p.
- Smyth, M.A., and Clapperton, C.M., 1986, Late Quaternary volcanic debris avalanches at Cotopaxi, Ecuador: *Revista Centro Interandino Americano de Fotointerpretación CIAF (Bogotá)*, v. 11, p. 24–38.
- Sodiño, L., 1877, Relación Sobre la Erupción del Cotopaxi Acaecida el Día 26 de Junio de 1877: Quito, Imprenta Nacional, 40 p.
- Sparks, R.S.J., 1986, The dimensions and dynamics of volcanic eruption columns: *Bulletin of Volcanology*, v. 48, p. 3–15, doi: 10.1007/BF01073509.
- Sparks, R.S.J., Bursik, M.I., Ablay, G.J., Thomas, R.M.E., and Carey, S.N., 1992, Sedimentation of tephra by volcanic plumes: Part 2. Controls on thickness and grain-size variations of tephra fall deposits: *Bulletin of Volcanology*, v. 54, p. 685–695, doi: 10.1007/BF00430779.
- Stübel, A., 1897, *Die Vulkanberge Ecuadors*: Berlin, A. Asher, 79 p.
- Takada, A., 1999, Variations in magma supply and magma partitioning: The role of tectonic settings: *Journal of Volcanology and Geothermal Research*, v. 93, p. 93–110, doi: 10.1016/S0377-0273(99)00082-7.
- Thorarinnsson, S., 1944, *Petrokronologiska Studier pa Island*: *Geographes Annuales Stockholm*, v. 26, p. 1–217.
- Velasco Juan de, S.J., 1844, *Historia del Reino de Quito en la America Meridional*: Quito, Imprenta Nacional, Historia Antigua, 3 volumes, 270 p.
- Vlastélic, I., Deniel, C., Bosq, C., Telouk, P., Boivin, P., Bachelery, P., Famin, V., and Staudacher, T., 2009, Pb isotope geochemistry of Piton de la Fournaise historical lavas: *Journal of Volcanology and Geothermal Research*, v. 184, no. 1–2, p. 63–78, doi: 10.1016/j.jvolgeores.2008.08.008.
- von Humboldt, A., 1837–1838, *Geognostische und physikalische Beobachtungen ueber die Vulkane des Hochlandes von Poggendorffs*: *Annalen der Physik und Chemie*, v. 40, p. 161–193 and v. 44, p. 193–219.
- von Humboldt, A., 1799–1804, *Briefe aus Amerika*: Berlin, Akademie-Verlag, p. 176–179.
- Wadge, G., Walker, G.P.L., and Guest, J.E., 1975, The output of Etna volcano: *Nature*, v. 294, p. 548–550, doi: 10.1038/294548a0.
- Whymper, E., 1892, *Viajes a Través de los Majestuosos Andes del Ecuador*: Salt Lake City, Utah, Peregrine Smith Books, 456 p.
- Wilson, L., and Walker, G.P.L., 1987, Explosive volcanic eruptions: VI. Ejecta dispersal in Plinian eruptions: The control of eruption conditions and atmospheric properties: *Geophysical Journal of the Royal Astronomical Society*, v. 89, p. 657–679.
- Wolf, T., 1878, Memoria Sobre el Cotopaxi y su Ultima Erupción Acaecida el 26 de Junio de 1877: Guayaquil, Imprenta de El Comercio, 48 p.
- Wolf, T., 1904, *Crónica de los Fenómenos Volcánicos y Terremotos en el Ecuador, con Algunas Noticias sobre otros Países de la América Central y Meridional, desde 1533 hasta 1797*: Quito, Ecuador, Imprenta de la Universidad Central, 121 p.
- Zúñiga, N., 1989, *Manuscritos Inéditos de Humboldt y la Ciencia Universal*: Ambato, Ecuador, Universidad y Sociedad, Universidad Técnica de Ambato, 288 p.

MANUSCRIPT RECEIVED 22 MARCH 2010

REVISED MANUSCRIPT RECEIVED 29 JULY 2010

MANUSCRIPT ACCEPTED 17 AUGUST 2010

Printed in the USA